DYNAMIC ROUTING OF UNMANNED AERIAL AND EMERGENCY RESPONSE TEAM INCIDENT MANAGEMENT

FINAL REPORT

February 2022

Hyoshin Park
North Carolina A&T State University

US DEPARTMENT OF TRANSPORTATION GRANT 69A3551747125

DISCLAIMER

The contents of this report reflect the views of the authors, who are responsible for the facts and the accuracy of the information presented herein. This document is disseminated under the sponsorship of the Department of Transportation, University Transportation Centers Program, in the interest of information exchange. The U.S. Government assumes no liability for the contents or use thereof.

1. Report No.	2. Government Accession No.	3. Recipient's Catalog No.
4. Title and Subtitle Dynamic Routing of Unmanned Aerial and Emergency Team Incident Management		5. Report Date Feb 2022 6. Source Organization Code Budget
7. Author(s) Park, Hyoshin, Sun Yi, Andy Alden		8. Source Organization Report No. CATM-2022-R2-NCAT
9. Performing Organization Name and Address Center for Advanced Transportation Mobility Transportation Institute 1601 E. Market Street Greensboro, NC 27411		10. Work Unit No. (TRAIS) 11. Contract or Grant No. 69A3551747125
12. Sponsoring Agency Name and Address University Transportation Centers Program (RDT-30) Office of the Secretary of Transportation–Research U.S. Department of Transportation 1200 New Jersey Avenue, SE Washington, DC 20590-0001		13. Type of Report and Period Covered Final Report: Feb 2019 –Feb 2022 14. Sponsoring Agency Code USDOT/OST-R/CATM
15. Supplementary Notes:		

16. Abstract. This study develops a proactive, dynamic emergency resource allocation framework to overcome the limitations of nearest methods while incorporating Unmanned Aerial Vehicles (UAVs) and crash dependencies. In the first part of study, the UAVs' role includes exploring uncertain traffic conditions, detecting unexpected events, and augmenting information gained from roadway traffic sensors. Resources are relocated in anticipation of future highway incidents and dispatched in response to a highway incident request. To find the optimal assignment of vehicles, the proposed model is solved using the Maximum Gain Method, further improved by incorporating an exploration heuristics. Overall, our model reports a 5.26% improvement in response time compared to the DCOP strategy. Aside from UAVs' assignment to incident locations, the UAVs provide enhanced transportation network coverage by reducing location assignments that result in overlapping observations. In the second part of study, a multivariate second-order Markov model estimates the probability of a secondary crash based on various primary incidents. This analysis will determine and identify if the probability of a secondary crash is higher at a specific location or higher due to a specific type of primary incident. Findings from our analysis can aid in developing countermeasures such as allowing emergency operators to allocate more resources to clear primary incidents quicker, or better prepare for secondary crashes based on the predicted probability of additional incidents.

Key Words
Ambulances; Disasters and emergency operations; Drones; Dynamic programming; Emergency response time; Incident management; Markov chains; Routing; Traffic crashes

17. Distribution Statement

Unrestricted; Document is available to the public through the National Technical Information Service; Springfield, VT.

18. Security Classif. (of this report)	19. Security Classif. (of this page)	20. No. of Pages	21. Price
Unclassified	Unclassified	58	…

Form DOT F 1700.7 (8-72) Reproduction of completed page authorized

TABLE OF CONTENTS

PART ONE: DYNAMIC ROUTING OF UAVs and ERVs

Executive Summary

Traditional incident management has dispatched resources to an immediate incident location without anticipation of near-future incidents. Previous distributed constraint optimization problem (DCOP) framework could allocate resources to highway incidents under static environments, simplifying dynamic behavior in distinct unconnected decisions. However, such an approach can not actively adapt to future changes in the environment and ignores dependencies between resource availability in near-future requests and the service time of each immediate incident request. The predictions of the environment and the resource availability in near-future requests should be considered through a look-ahead model when making decisions in the current time. This study develops a proactive, dynamic framework to overcome the above limitations and formulates the objective of the optimization problem to incorporate Unmanned Aerial Vehicles (UAVs). The UAVs' role includes exploring uncertain traffic conditions, detecting unexpected events, and augmenting information gained from roadway traffic sensors. Resources are relocated in anticipation of future highway incidents and dispatched in response to a highway incident request. To find the optimal assignment of vehicles, the proposed model is solved using the Maximum Gain Method, further improved by incorporating an exploration heuristics. Overall, our model reports a 5.26% improvement in response time compared to the DCOP strategy. Aside from UAVs' assignment to incident locations, the UAVs provide enhanced transportation network coverage by reducing location assignments that result in overlapping observations.

1 Introduction

Traffic Incident Management (TIM) programs have traditionally focused on reducing congestion and enhancing highway safety mainly through its Full-Function Service Patrols (FFSP)s program (fhw). Under the FFSP program, service patrol vehicles such as Emergency Response Vehicles (ERV)s are dispatched to perform tasks including traffic incident clearance, traffic control and scene management, and incident detection and verification. In this study, we assume a trained FFSP operator uses a fully equipped ERV capable of rapidly removing incident-involved automobiles or light trucks to a safe location without having to wait for a wrecker.

One of the main challenges facing the TIM program is the efficient deployment of the limited resources (i.e., ERVs) in response to a sequence of incident requests. A typical deployment goal is to minimize the overall response time of all ERVs to the incident scenes. To support this goal, TIM programs have conventionally assigned the next available and closest ERV to an incident scene and return to the depot after performing the task at the scene. However, this approach overlooks several important components that can improve the overall response time of ERVs to incident requests. First, to assign an ERV to a current incident request, the dispatcher at the Traffic Operations Center (TOC) may consider possible near-future incident occurrences and assign another ERV instead of the closest one to the current incident request. The closest ERV not served in the current request could be closer to the expected location of a near-future emergency, which may result in a lower overall response time of the ERVs to the sequence of incident requests. Second, the expected time and location of near-future incident occurrences has traditionally been assumed to be independent of past and current incidents. However, past and current incidents may provoke a future incident. For example, every minute a primary incident is left uncleared, there is an increased chance of a secondary incident due to reduced speed and rubbernecking on the travel lane of the original incident. By considering this dependency, we can better predict near-future incident occurrences and improve the assignment performance of ERVs. Third, suppose the expected available time of a busy ERV is earlier than the expected occurrence time of the next incident. In that case, we can include that ERV as one of the available ERVs for the next assignment. On the other hand, if the expected available time of a busy ERV is later than the expected occurrence time of the next incident, then we remove that ERV during the next assignment window. By considering the

availability of the ERVs based on the expected clearance time of incidents in the ERV deployment model, we avoid making short-sighted ERV assignments.

A few studies have attempted to address the aforementioned challenges. For example, deploying emergency vehicles can be solved by a constraint satisfaction model with hard constraints (e.g., a time window to respond and clear an incident) (Steinbauer and Kleiner, 2012). Unfortunately, as with constraint satisfaction models, a single constraint violation causes the model to fail to find a solution, making it primarily unsuitable for many real-world implementations. Another notable example is the online optimization model that considers stochastic nature of event occurrences, duration of emergencies, and busy time of emergency vehicles (Park et al., 2019). The online optimization model receives a sequence of emergency calls and performs an immediate action (dispatch decision) in response to each request. However, there was no direct framework for relocation decisions that can be made in parallel with dispatch decisions. If done properly, relocation of free ERVs based on expected near-future emergencies can greatly improve the response time in TIM.

While considering the above-mentioned components will improve the deployments of ERVs in TIM, emerging technologies such as Unmanned Aerial Vehicles (UAVs) are providing new opportunities to enhance operations in TIM. In particular, the Next-Generation (NextGen) TIM seeks to integrate new and emerging technology (e.g., UAVs), tools, and training to improve incident detection and safety response and reduce clearance times at roadway crashes (NEX). Under revised Federal Aviation Authority (FAA) regulations that accommodate UAVs' advanced operations, UAVs and ERVs can coordinate their deployments in response to an incident to provide more benefits in TIM programs. The role of UAVs in heterogeneous vehicle-team yields three key enhancements. First, aerial view on the possible route of ground vehicles can update the availability of the freeway shoulder lanes, allowing an ERV to safely travel at as high speed as possible. Second, sparse freeway sensor network cannot accurately estimate the location and speed of non-recurring congestion (e.g., shockwave). Aerial monitoring of moving shockwave can help estimation of the true impact of an incident. Third, real-time information of an incident scene can be gathered by monitoring the clearance progress from tethered UAVs. The previous online optimization model (Park et al., 2019) supports a single-type vehicle team and can not coordinate UAVs and ERVs in TIM. Deployment of UAVs and ERVs must be carefully coordinated to provide more benefit in TIM, including ERVs

use of route-to-incident information from UAVs for a safe and fast response to an incident scene (see Figure 1).

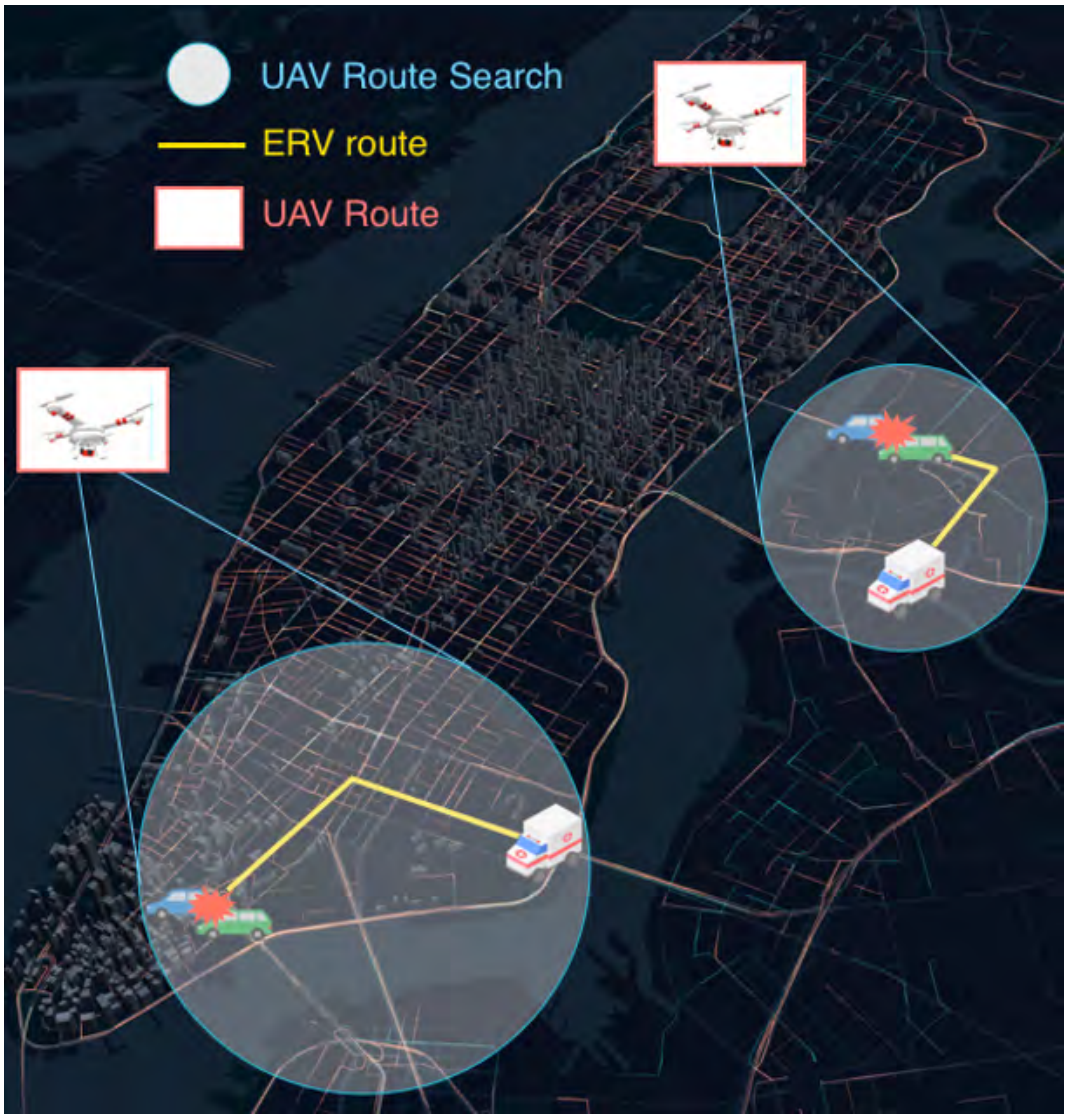

Figure 1: UAVs and ERVs in Traffic Incident Management

For many reasons, the distributed constraint optimization framework presents an attractive problem-solving approach for heterogeneous agents in TIM. First, the distributed constraint optimization framework relaxes the hard constraints to find the optimal deployment solution rather than solving the optimal deployment solution by fulfilling a set hard constraint (e.g., constraint satisfaction model). This makes it more flexible for modeling real word problems, especially for large agent networks. Second, in networks where it is not feasible to set up a centralized command station (e.g., TOC), the distributed framework can utilize the onboard computing units on each agent

(i.e., ERV and UAV), and with little communication overhead, find system optimal deployment solutions. For networks with centralized command stations, the distributed framework can create multiple virtual agents whose concurrent activities are then simulated at the central command station. Third, the problem-solving activities are distributed among the agents, making them robust against failure when any one or more agent fails. In other words, since knowledge of constraints is inherently distributed among the agents, each agent in the deployment fleet can autonomously decide the best solution sharing as little information as possible. In the case of constraint satisfaction, the model requires one central agent to have knowledge of all the constraints making it more susceptible to failure when that central agent fails. Fourth, the distributed framework can exploit potential parallelism in constraint networks that define the partially connected sub-problems of the heterogeneous agents in TIM. For example, by carefully connecting the problem of deploying ERVs and UAVs, the ERVs can use route-to-incident information from UAVs for a safe response to incident scenes.

Previous studies on distributed constraint optimization (Modi et al., 2005a; Yeoh and Yokoo, 2012) have proposed models to integrate ERVs and UAVs in a multi-agent TIM problem (Darko et al., 2021a,b). However, this model assumed a static environment, simplifying dynamic behaviors of traffic and events changing by time. A myopic resource allocation decision that does not consider the sequence of dependent events can not proactively adapt to changes in the environment over multiple time stages. Also, the availability of emergency resources for near-future emergencies was not considered that could be estimated based on the service time of current request. The predictions of the environment and the resource availability in a future time should be considered through a look-ahead model when making decisions in response to the current request. This paper extends the distributed constraint optimization for allocating ERVs and UAVs developed in a multi-agent TIM. We develop the distributed allocation of aerial and ground emergency resources by predicting and proactively responding to dynamic changes to the traffic network. In addition, we directly consider the relocation of free ERVs based on the expected location of near-future emergencies in parallel with the dispatch decisions based on current incident requests. This unified approach will focus on maximizing a set of utility constraints to improve the overall benefit of the assignments for the traffic operations system during recurring and non-recurring congestion. The motivating domain is modeled as the Proactive Dynamic Routing Of uNmanned-aerial and Emergency Team Incident

Management (P-DRONETIM). We highlight the contributions of this paper as follows:

- A proactive distributed decision-making framework for deploying emergency resources in a multi-agent TIM problem to minimize the time needed to respond to a sequence of emergency requests.
- A unified approach is introduced to relocate free ERVs based on the expected location of near-future emergencies in parallel with dispatching policies based on current incident requests.
- The ERVs are assumed to use the freeway shoulder to get to the incident scene. When a UAV observes the route-to-incident location (i.e., freeway shoulder), the percentage improvement in response time (or speed) of the ERV to incident location is based on the level of risk on the freeway shoulder (e.g., due to debris or disabled vehicles on the shoulder).
- UAV aerial monitoring of moving shortwaves in the vicinity of the incident updates the estimate of the true impact of the incident (total delay).
- Compare the DCOP and PD-DCOP approaches to ERV deployment through experimentation and simulations on a prototype network abstracted with data of traffic flow parameters.

2 Literature Review

Most highway incident management studies have focused on allocating a set of emergency vehicles under a single-period emergency service allocation model (Yin, 2006, 2008), with few studies extending to a multi-period (Park et al., 2016). A single-period emergency service allocation model is myopic and fails to consider the near-future request's impact on improving the immediate request's decision. In deciding how to allocate emergency vehicles, the relocation and dispatch of the emergency vehicles have been developed as separate models without considering the interdependencies between the two decisions (Park et al., 2019; Darko et al., 2021a). However, developing a connection between these two decisions will provide an efficient relocation decision that will improve the overall response time during dispatch. Concerning the use of emergency vehicles, there has been a lack of focus on developing a framework to integrate UAVs to support the operations of emergency vehicles in highway incident management. Under revised FAA regulations

that accommodate UAVs advanced operations, a significant opportunity is presented for policy improvement in highway incident management. UAVs can provide enhanced information about the incident scene and aid the emergency vehicles to arrive at the incident site at full speed.

A DCOP framework (Modi, 2003) for incident management moves the focus from emergency vehicle allocation to a heterogeneous vehicle team. The resource allocation problem in traffic incident management has been modeled under DCOP to automate the activities of a heterogeneous vehicle team (ERVs and UAVs) under static conditions (Darko et al., 2021a). Research on DCOP under stochastic uncertainty shows that network uncertainty can be reduced through multi-agent collaborative sampling (Léauté and Faltings, 2011). Multi-agent coordination has been successfully used to efficiently explore unknown environments using the probabilistic multi-hypothesis tracker (PMHT) technique (Cheung et al., 2010). Using the Adopt polynomial-space algorithm, DCOP has been shown to achieve globally optimal solutions under asynchronous task execution while achieving high computational efficiency (Modi et al., 2005a; Modi, 2003). While a DCOP can handle a single-period efficiently, it fails to accommodate the interdependencies in a multi-period problem. To accommodate the dynamically changing environment and the dependencies in different stages, this study models the resource allocation in the traffic incident management problem as the P-DRONETIM. P-DRONETIMs are able to directly model interdependencies and the possible changes in a multi-stage problem. Compared to previous studies, we consider a heterogeneous vehicle fleet under a unified framework for dispatch and relocation decisions to accurately capture interdependencies in the decisions. The probability of incident occurrences at a location for different times of the day is achieved using historical incident characteristics of the given area. A multi-stage decision is developed to consider the near-future availability of emergency vehicles and anticipate future events. Different solution techniques have been provided in literature that focuses on optimizing different metrics such as message count, cost, and cycles. This includes complete algorithms that find the optimal solutions but usually fail in large and complex environments (Modi et al., 2005a), and incomplete techniques such as Maximum Gain Method (MGM) that provide high-quality solutions, especially for systems with large constraints density (Farinelli et al., 2014). The MGM is applied to P-DRONETIM in this study.

3 Preliminaries

3.1 Approach Overview

The proactive dynamic version of DCOP is defined by a tuple $\langle \mathbb{A}, \mathbb{X}, \mathbb{D}, \mathbb{F}, T, \alpha, c, \gamma, p_Y^0 \rangle$ where $\mathbb{A} = \{A_1, A_2, \ldots, A_n\}$ is a finite set of agents (ERVs and UAVs), $\mathbb{X} = \{X_1^t, X_2^t, \ldots, X_m^t\}$ is a finite set of variables for each time stage $t \in T$ (with m≤n), $\mathbb{D} = \{D_1, D_2, \ldots, D_m\}$ is a finite set of domain values for each variable, $\mathbb{F}$ is a finite set of constraints between variables, T is a finite horizon in which the agents can change their assignment, α maps variables to vehicles, $c \in \mathbb{R}^+$ is a switching cost, defined as the cost associated with changing the assignment of a variable from one time stage to the next, $\gamma \in [0, 1)$ is a discount factor, which represents the difference in importance between future and present cost, and $p_{\mathbf{Y}}^0 = \left\{p_y^0\right\}_{y \in \mathbf{Y}}$ is a set of initial probability distributions for the random variables. Each variable X_i^t is held by an agent who chooses a value to assign it from the finite set of values D_i; Each constraint $\mathcal{C} \in \mathbb{F}$ is a function $C : D_{i_1} \times D_{i_2} \times \ldots \times D_{i_k} \rightarrow \mathbb{R}_+ \cup \{0\}$ that maps assignments of a subset of the variables to a non-negative cost. The cost of a full assignment of values to all variables is computed by aggregating the costs of all constraints. Addition is the aggregation operator most commonly considered so that the total cost is the sum of the constraint costs, but other operators, such as the maximum, have also been considered (Modi et al., 2005b; Schiex et al., 1995). The goal of the proactive dynamic DCOP is to find a sequence of T+1 assignments to variables with minimum total cost over the entire horizon T. Vehicles operate distributedly and need to decide their assignment locations at different times of the day to minimize the response time to freeway incidents. Control is distributed to the agents who can only assign values to variables that they hold. Furthermore, agents are assumed to know only of the constraints involving variables that they hold, thereby distributing knowledge of the structure of the DCOP. In order to coordinate, agents must communicate via message passing. It is commonly assumed that agents can only communicate with agents who hold variables constrained with their own variables, called their neighbors (Modi et al., 2005b; Pearce and Tambe, 2007; Yokoo and Hirayama, 2000; Zhang et al., 2003). While transmission of messages may be delayed, it is assumed that messages sent from one agent to another are received in the order that they were sent.

3.2 Problem Domain

We develop the P-DRONETIM model by considering the following problem domain: UAVs provide information about a defined region once assigned to a given location. We define an overlapping region for each UAV observation regarding the other UAVs by determining the number of UAVs occupying their neighbor locations at the same time. The number of occupied neighbor locations is used to estimate the overlapping observation region. The overlapping region defines a reduction in benefit for UAVs assigned in the same vicinity at the same time.

This study deals with a type of ERV on freeways. e.g., CHART (Coordinated Highways Action Response Teams) that provide rapid removal of incident-involved vehicles from the travel lanes. The ERVs respond to an incident request using enhanced route information from UAVs if both ERV and UAV are simultaneously assigned to the incident location. UAVs also provide information about the incident scene on highways. The Traffic Incident Management Handbook (Farradyne, 2000) describes an incident as “any non-recurring event that causes a reduction of roadway capacity or an abnormal increase in demand." Under this description, events such as traffic crashes, disabled vehicles, spilled cargo, highway maintenance and reconstruction projects, and special non-emergency events are classified as an incident. The illustrations of incidents in this study will focus mainly on traffic crashes.

Our unified location assignment model consists of a relocation decision to anticipate near-future incidents and a dispatch decision in response to an immediate incident request. While the current emergency vehicle relocation plans adopt a fixed identical pattern, the probability of an incident occurring at different times of the day (e.g., morning peak hours) should be considered when making relocation decisions. We define the probability of highway incidents for three planning stages concerning different times of the day: morning peak hours, normal hours, and evening peak hours. The highway incident distribution is estimated from historical data of crashes at different locations and times. For instance, the total crash frequency for a given intersection during the morning peak hours can be used to estimate the probability of a crash occurring at the intersection during that period. The reward of a relocation decision is developed as a random variable that depends on the probability of incident occurrence, possible time of incident occurrence, response time, and the possible severity of the incident at that location. With the help of advanced traveler

information system and incident information system (e.g., https://drivenc.gov), more accurate data will be available on time for the assignment to be properly made.

The dispatch decisions are defined for different times of the day, covering the three planning stages. For instance, $0 \dots n$ = morning peak hours, $n \dots n_1$ = normal hours, and $n_1 \dots T$ = evening peak hours. The reward of a dispatch decision is based on the incident severity, estimated delay savings, and response time to the incident. The goal is to find a robust solution to possible changes, anticipating future highway incidents.

4 P-DRONETIM Model

In the P-DRONETIM model, vehicles hold the variables $X^t_{a\in\mathbb{A}} \in \mathbb{X}$, where $a \in \mathbb{A}$ is the set of ERVs and UAVs and $t \in T$ is the different times of the day. The domain $D_{X_{a\in\mathbb{A}}}$ for the variables $X^t_{a\in\mathbb{A}}$ is the set of possible observation location $j \in J$. For example, $UAV1$ holding variable X^1_{UAV1} has a domain given by $D_{X_{UAVn}} = \{1, 2, 3, ..., J\}$. For each time of day $t \in T$, a vehicle $a \in \mathbb{A}$ selects a possible assignment location $j \in J$ for its decision variable given by $X^t_{a\in\mathbb{A}} = \{X^0_a, \dots, X^T_a\}$.

4.1 Vehicle Assignment Constraints

A UAV and ERV cannot be assigned to two locations at the same time of day. This is represented by the following relations:

$$\forall A^t_{UAVn}, B^t_{UAVn} \in X^t_{UAVn} \times X^t_{UAVn}, A \neq B \Rightarrow A^t_{UAVn} \neq B^t_{UAVn}$$

$$\forall A^t_{ERVm}, B^t_{ERVm} \in X^t_{ERVm} \times X^t_{ERVm}, A \neq B \Rightarrow A^t_{ERVm} \neq B^t_{ERVm}$$

4.2 Vehicle Dispatch Reward Definitions

The following reward functions are developed to coordinate the assignment of the heterogeneous vehicle team.

4.2.1 Single Vehicle Coordination Reward (UAVs)

The reward $f : D_{X_{UAVn}} \rightarrow \mathbb{R}$ for dispatching $UAVn$ to location j is described by the following:

- The severity ω of the highway incident at location j. The severity is proportional to the capacity reduction (i.e., the number of lanes closed rising from the incident)(Park and Haghani, 2016a).

- The reduction in uncertainty of estimated traffic flow parameters such as traffic flow rate q in the region of the assignment location j until capacity is restored to normal condition. We develop this as a parameter ρ_j equivalent to the uncertainty reduction in traffic flow rate q in the region of location j.

We discount the reward by the response time rt to the assigned location j. The reward function is defined as

$$f\left(X^t_{UAVn}\right) = (\alpha * \rho_j + \beta^{\omega}_j) * (\frac{1}{rt}), \tag{1}$$

where α and β^{ω}_j are constants describing the traffic state and the severity of the incident, respectively.

4.2.2 Single Vehicle Coordination Reward (ERVs)

The reward $f : D_{X_{ERVm}} \rightarrow \mathbb{R}$ for dispatching $ERVm$ to location j is described by the following:

- The severity ω of the highway incident at location j. In the case of relocation in anticipation of future incidents, the probability and severity of the incident is considered.

- An estimated delay saving $\mathcal{D}$ at location j by assigning $ERVm$ at time t.

The reward function is defined as

$$f\left(X^t_{ERVm}\right) = (\mathcal{D}^m + \beta^{\omega}_j), \tag{2}$$

where $\mathcal{D}^m$ is proportional to the response time rt of $ERVm$ to location j.

4.2.3 Binary Vehicle Coordination Constraints

The role of the UAV in the heterogeneous vehicle team is to explore unknown traffic conditions, unexpected situations on roads, and enhance prior information from loop detectors, automatic vehicle identification detectors, probe vehicle data, and other sensors. Once the traffic information

center provides such information, the information collected from a UAV will enable an ERV to reach the incident locations with reduced delay. The reward for an assignment between any ERV and UAV pair is given by

$$f\left(X^t_{ERVm}, X^t_{UAVn}\right) = \begin{cases} \alpha * \rho_j & \text{if } X^t_{UAVn} == X^t_{ERVm} \\ 0 & \text{otherwise} \end{cases} \tag{3}$$

To optimize the monitoring of locations by UAVs and manage the limited resources, we define a coordination constraint for an overlapping surface area $\Omega\left(X^t_{UAVa}, X^t_{UAVb}\right)$ between any two locations written as

$$f\left(X^t_{UAVa}, X^t_{UAVb}\right) = \begin{cases} -\infty & \text{if } X^t_{UAVa} == X^t_{UAVb} \\ -\Omega\left(X^t_{UAVa}, X^t_{UAVb}\right) & \text{otherwise} \end{cases} \tag{4}$$

The overlapping surface area defines a reduction in benefit for UAVs assigned in the same vicinity. Under conditions of limited resources, the ERVs' role is to coordinate their local decision-making to ensure that one ERV is assigned to a location at any time. This is given by the coordination constraint representing the assignment of ERVs to different locations:

$$f\left(X^t_{ERVa}, X^t_{ERVb}\right) = \begin{cases} -\infty & \text{if } X^t_{ERVa} == X^t_{ERVb} \\ 0 & \text{otherwise} \end{cases} \tag{5}$$

The preferred coordination of location assignment is such that UAVs and incident location are the same in order for the ERV to utilize information from the UAV.

In the case of relocation in anticipation of near-future incidents, we define a random variable y_j whose reward function is dependent on the probability $p(\omega)$ and severity β^{ω}_j of the incident at time t.

4.3 Vehicle Relocation Reward Definitions

For the set of possible incident locations $j \in J$, we define $P^t_{y_j}(\omega)$ as the probability of incident severity $\omega \in \Omega$ occurring at time t. The reward of a relocation to j at time t is given by the expected benefit discounted by the response time to location j.

$$f_{y_j} = \left(\sum_{\omega \in \Omega} p^t_{y_j}(\omega) \cdot \beta^{\omega}_j \right) * \frac{1}{rt} \tag{6}$$

We define $\mathbf{T}_{y_j}(\omega', \omega) = P(y^t_j = \omega | y^{t-1}_j = \omega')$, as a transition function, where $y^t_j = \omega \in \Omega_{y_j}$ denotes the incident severity of the variable y_j at time stage t and $y^{t-1}_j = \omega' \in \Omega_{y_j}$ denotes the incident severity of the variable y_j at time stage $t-1$. For the different times of the day $t \in T$, the sum of the probabilities of variable y_j at location $j \in J$ is one, written as

$$\sum_{t=1}^{T} \mathbf{T}_{y_j}(\omega', \omega) = 1, \quad \forall j \in J. \tag{7}$$

The probability of the random variable y_j to take value ω at time t is given as

$$p^t_{y_j}(\omega) = \sum_{\omega' \in \Omega_{y_j}} \mathbf{T}_{y_j}(\omega, \omega') \cdot p^{t-1}_{y_j}(\omega'). \tag{8}$$

4.4 Vehicle Energy Constraint

The energy required $\mathcal{E}^a_j : D_{X_a} \rightarrow \mathbb{R}$ by vehicle $a \in \mathbb{A}$ in moving from an initial location i to the currently assigned location j is given by the energy consumed when vehicle a moves to location j

$$\mathcal{E}^a_j = k * |d_{i,j}| + K_j, \tag{9}$$

where k is the energy consumed by vehicle a per unit distance. $|d_{i,j}|$ is the distance between initial location i and the currently assigned location j. In this work, $|d_{i,j}|$ is defined as the Euclidean distance and shortest city block distance for UAVs and ERVs respectively. We define K_j as a constant for an extra energy consumed due to detours by ERVs or for observing the region of location j by UAVs. The state of the vehicle a at location j is given by the available energy A_j at that location, represented by (j, A_j). The total energy required for all location assignments of vehicle a must not exceed the vehicle's total available resource A.

$$\sum_{j \in J} \mathcal{E}^a_j \leq A, \quad \forall a \in \mathbb{A} \tag{10}$$

This constraint can be relaxed to assume the vehicle have sufficient energy for assignments at all time.

4.5 Switching Cost

In this work, we develop a varying switching cost when a location decision is changed for vehicle $a \in \mathbb{A}$ between time stages written as

$$c\left(X_a^t, X_a^{t+1}\right) = \begin{cases} c^{(t \to t+1)} & \text{if } X_a^t \neq X_a^{t+1} \\ 0 & \text{otherwise} \end{cases} \tag{11}$$

Let $x^{(t \to t+1)}$ be the response time (travel time) required to move from location i at time t to location j at time $t+1$, then the normalized response time defining the varying switching cost $c^{(t \to t+1)}$ is calculated as:

$$c^{(t \to t+1)} = \frac{x^{(t \to t+1)} - \min(x)}{\max(x) - \min(x)} \tag{12}$$

where $\min(x)$ and $\max(x)$ is the minimum and maximum response time between any two locations in the network. The goal of PD-DCOP is to find a sequence of T+1 assignments $\mathbf{X}^*$ for all the decision variables in $\mathbb{X}$.

$$\mathbf{X}^* = \underset{\mathbf{x}=\langle \mathbf{x}^0, \ldots, \mathbf{x}^T \rangle \in \Sigma^{T+1}}{\operatorname{argmax}} \mathcal{F}^T(\mathbf{x}) \tag{13}$$

where

$$\begin{aligned} \mathcal{F}^T(\mathbf{x}) = & \sum_{t=0}^{T-1} \gamma^t \left[\mathcal{F}_x^t\left(\mathbf{x}^t\right) + \mathcal{F}_y^t\left(\mathbf{x}^t\right)\right] \\ & - \sum_{t=0}^{T-1} \gamma^t \left[c \cdot \Delta\left(\mathbf{x}^t, \mathbf{x}^{t+1}\right)\right] \\ & + \tilde{\mathcal{F}}_x\left(\mathbf{x}^T\right) + \tilde{\mathcal{F}}_y\left(\mathbf{x}^T\right) \end{aligned} \tag{14}$$

where Σ is the assignment space for the decision variables of the P-DRONETIM at $t \in T$. $\mathcal{F}_x^t$ and $\mathcal{F}_y^t$ in (14) are the reward functions involving a dispatch and relocation decisions at time t.

$$\begin{aligned} \mathcal{F}_x^t(\mathbf{x}) &= \sum_{f_j \in \mathbb{F} \setminus \mathbb{F}_Y} f_j\left(\mathbf{x}_j\right), \\ \mathcal{F}_y^t(\mathbf{x}) &= \sum_{\omega \in \Omega_{y_j}} f_{y_j}\left(\mathbf{x}_j|_{y_j=\omega}\right) \cdot p_{y_j}^t(\omega) \end{aligned} \tag{15}$$

$$\tilde{\mathcal{F}}_x(\mathbf{x}) = \frac{\gamma^T}{1-\gamma}\mathcal{F}_x^T(\mathbf{x}),$$
$$\tilde{\mathcal{F}}_y(\mathbf{x}) = \sum_{\omega \in \Omega_{y_j}} \tilde{f}_{y_j}\left(\mathbf{x}_j|_{y_j=\omega}\right) \cdot p_{y_j}^T(\omega) \tag{16}$$

$$\tilde{f}_{y_j}\left(\mathbf{x}_j|_{y_j=\omega}\right) = \gamma^T \cdot f_{y_j}\left(\mathbf{x}_j|_{y_j=\omega}\right)$$
$$+\gamma \sum_{\omega' \in \Omega_{y_j}} \mathbf{T}_{y_j}(\omega, \omega') \cdot \tilde{f}_{y_j}\left(\mathbf{x}_j|_{y_j=\omega'}\right) \tag{17}$$

5 Solution Approach

The choice of local search over complete search for PDRONETIM is justified by the conventional standard arguments for adopting local over complete search namely; time constraints and the scale of problems that complete algorithms can efficiently handle. Furthermore, the following PDRONETIM qualities support the use of a local search algorithm:

- Emergency vehicles (ERVs and UAVS) would have to assume every feasible position for a complete search, which is not feasible for large search spaces as seen in traffic incident management.
- Because changes that occur during the search for the best solution render the calculated solution outdated, dynamic modifications reduce the time that agents have to implement a complete algorithm.
- While complete search is expected to find the best solution, this can be computationally expensive with no guarantees on the degree of coverage while the best final configuration is being computed. The algorithm must maintain reasonable coverage while adjusting to changes in the problem (Mailler, 2005; Jain et al., 2009).

Our solution is based on the local search algorithm Maximum Gain Method (MGM)(Maheswaran et al., 2006). The expected incident duration, given by the sum of the expected response time and clearance time, is used to estimate the availability of the resource for the next time stage. Therefore, not all possible assignment combinations will be feasible. For example, assume ERV1 is to be relocated from location i to j at 9:00 am. If the expected incident duration for the previous request

location i at 8:00 am exceeds 9:00 am, then ERV1 is unavailable for relocation to j at 9:00 am. In this case, assignments $X_{ERV1}^{8:00am} = X_{ERV1}^{9:00am} = i$. The main steps developed for the solution approach are as follows:

Step-1: Make Initial random assignments while enforcing the available resource constraint for all vehicles for all time periods. The vehicle initializes its information of the other vehicles' assignment for all time stages in the network (initial is null).

Step-2: Each vehicle updates their information about the neighboring vehicles' assignment by receiving the current assignment of the neighbors for all time stages.

Step-3: Each vehicle computes its current utility for each time stage for the current assignment combination while considering its information on the neighboring vehicles.

Step-4: Each vehicle searches all feasible assignment for all time stages considering the vehicle's initial location at $t = 0$ while enforcing the available resource constraint. The combination with the maximum cumulative utility is determined.

Step-5: Each vehicle then calculates its gain by finding the difference at each time stage between the current assignment utility and the assignment combination with the maximum cumulative utility.

Step-6: Each vehicle sends and receives the neighbor's gain (ERV to ERV, and UAV to UAV). The vehicles then update the locations of the current assignments at the time stages that have a gain greater than zero and greater than the maximum gain of the neighbors. Thus, the vehicle assigns its best location for these time stages as its current location and restarts step 2 by sending a message that contains its new locations to its neighbors.

6 Scenarios and Experiments

We perform experiments for a prototype network abstracted with travel time and traffic flow rate data of an existing highway network. The network has nine intersections representing the possible crash locations. The probability of a crash type occurring at a given location during the planning stages is estimated from historical crash data at intersections.

Figure 2 shows the frequency of different crash types for morning peak hours, normal hours, and evening peak hours at intersection 5 of the network. An Incident request can occur at defined periods, representing the time of day. We generate a sequence of incident requests at different times

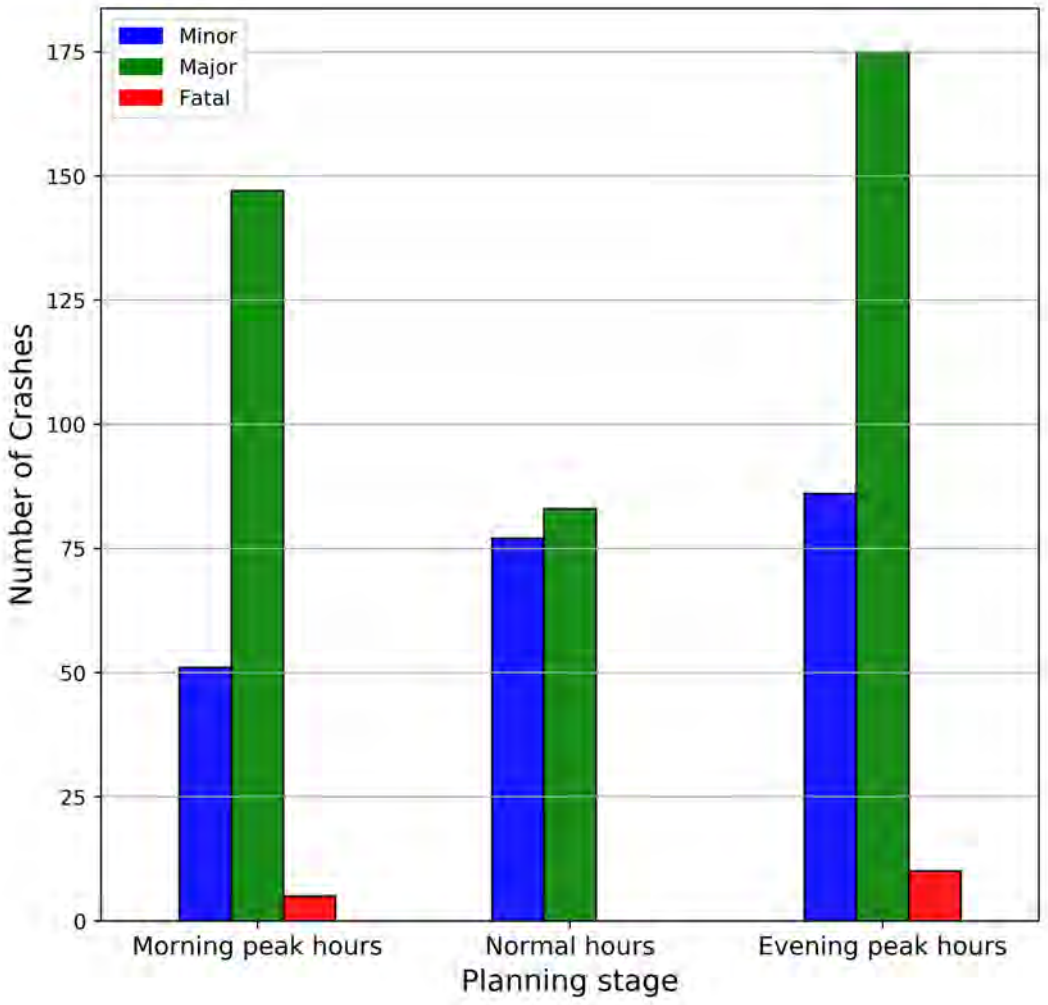

Figure 2: Incident severity distribution for three planning stages at intersection 5.

by randomly drawing the time of crash and location from the range of the times and the possible crash locations separately. This process allows us to generate real-world scenarios such as crashes at different locations at the same time. Each crash is given a random severity number drawn from a uniform distribution between 1 and 3 representing a minor, major, and fatal crash.

The estimated clearance time for each incident severity is randomly drawn from a distribution as shown in Figure 3. A dispatch and relocation decision are made depending on the availability of the ERVs at the time. We assume each ground emergency vehicle and unmanned aerial vehicle is given an initial location following current practice. In the case of a UAV relocation decision, we assume an aerial surveillance plan for the highway network that maximizes information collected about the transportation network. In order words, the relocation decision will reduce overlapping

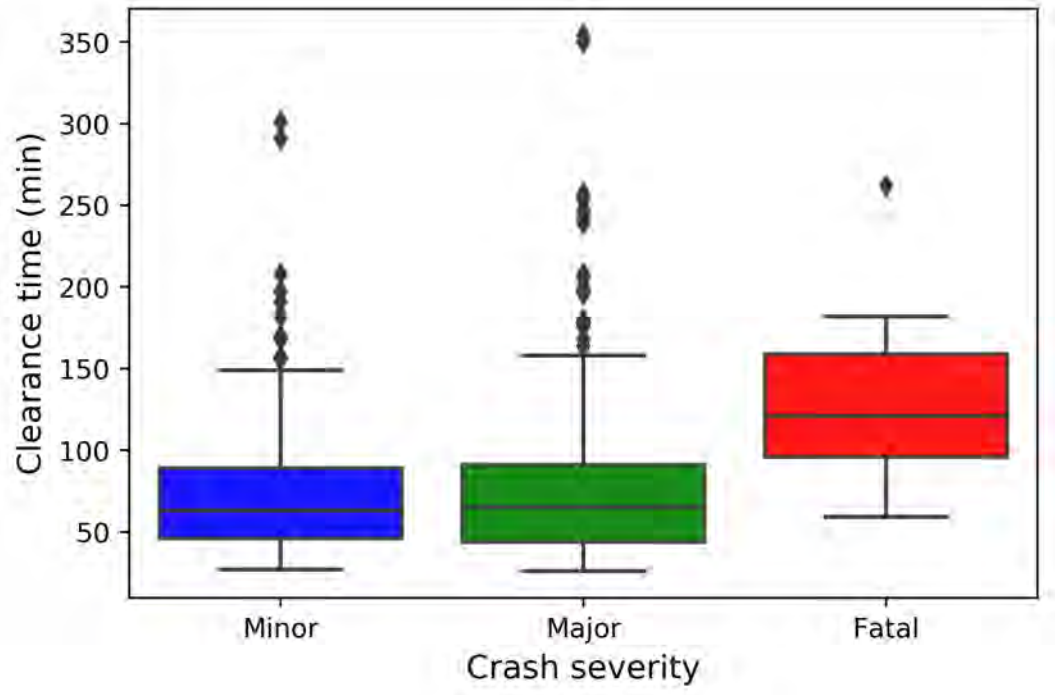

Figure 3: Distribution of clearance time for different incident severity.

observations. For simplicity, we assume that UAVs maintain a fixed altitude during their flights and cover a given region in the network once assigned to a given location. Vehicles can communicate with each other using a low-bandwidth Radio frequency.

Two main scenarios are provided to test the robustness of our model. In the first scenario, we vary the number of incident requests while keeping the number of vehicles constant. In the second scenario, we vary the number of vehicles in the network while keeping the number of incident requests constant. A summary of the scenarios is presented in Table 1.

Table 1: Distribution of scenarios in the network.

Scenario 1		
Number of requests	Number of ERVs	Number of UAVs
3	2	2
5	2	2
9	2	2
Scenario 2		
9	2	2
9	3	3
9	4	4

7 Evaluation

Preliminary results of the two scenarios are presented for the MGM approach to P-DRONETIM. The MGM algorithm is highly exploitative, preventing the exploration of other possible solutions. We introduce exploration by applying the Distributed Stochastic Algorithm (DSA) (Tel, 2000) to the P-DRONETIM model. In DSA, a vehicle's assignment to a location is accepted if a specified probability threshold has been satisfied, introducing randomness in selecting other feasible solutions.

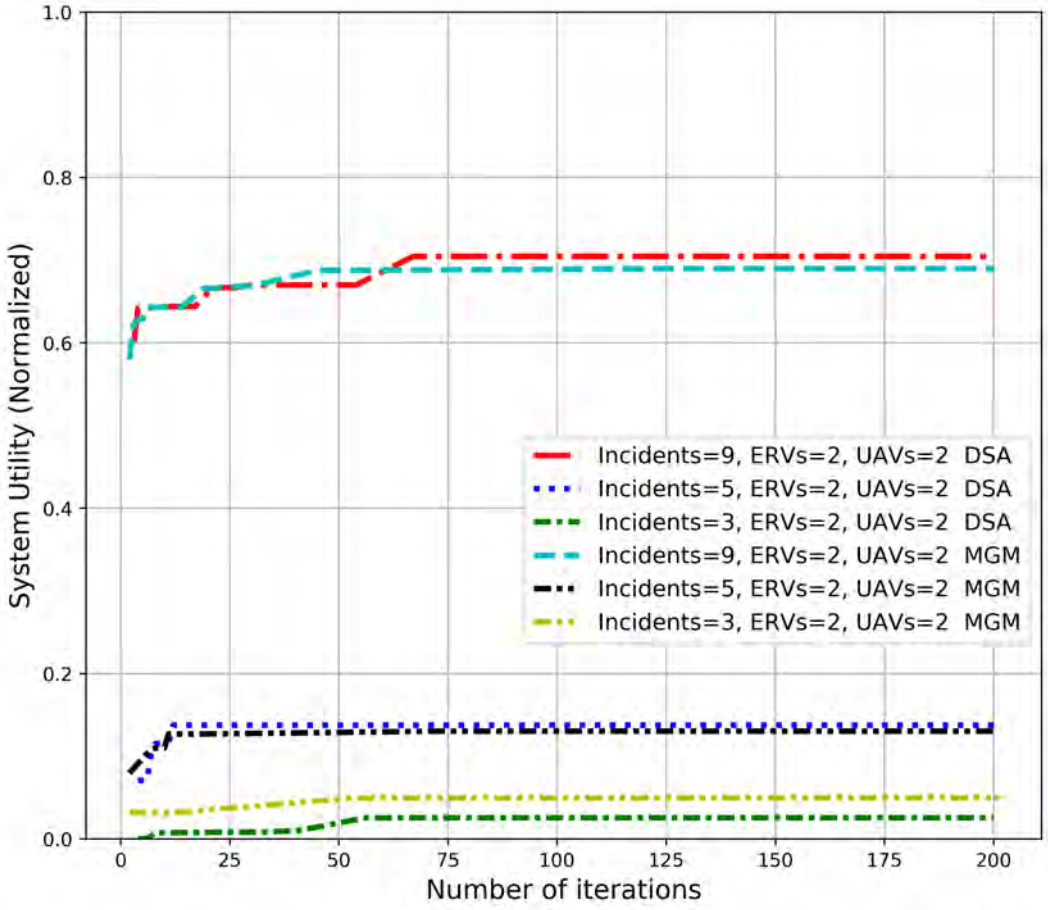

Figure 4: Convergence of MGM and DSA (p=0.5) for varying incident number request with fixed number of vehicles.

The results in Figure 4 show the effects of varying incident requests at different times on the quality and convergence to an optimal solution, assuming a fixed number of vehicles. In the case of 5 incident requests, we observe a higher utility when compared to 3 requests since the vehicles can clear more incidents. The same trend is seen when the incident requests are increased to 9. Aside

from the number of requests influencing the utility, the severity of the incidents also plays a role. The higher the severity, the more benefits are gained when the incident is cleared. For instance, with different severities for nine requests, more benefit is achieved depending on the cleared incidents. For all cases, MGM and DSA algorithms converged after a few iterations. The number of vehicles used in the above scenario may not provide the most benefit for the system. Resources may not be readily available for concurrent and new requests if the resource is already in service of the current dispatch assignment. We see this clearly when we vary the number of vehicles for a fixed incident request, as seen in scenario 2.

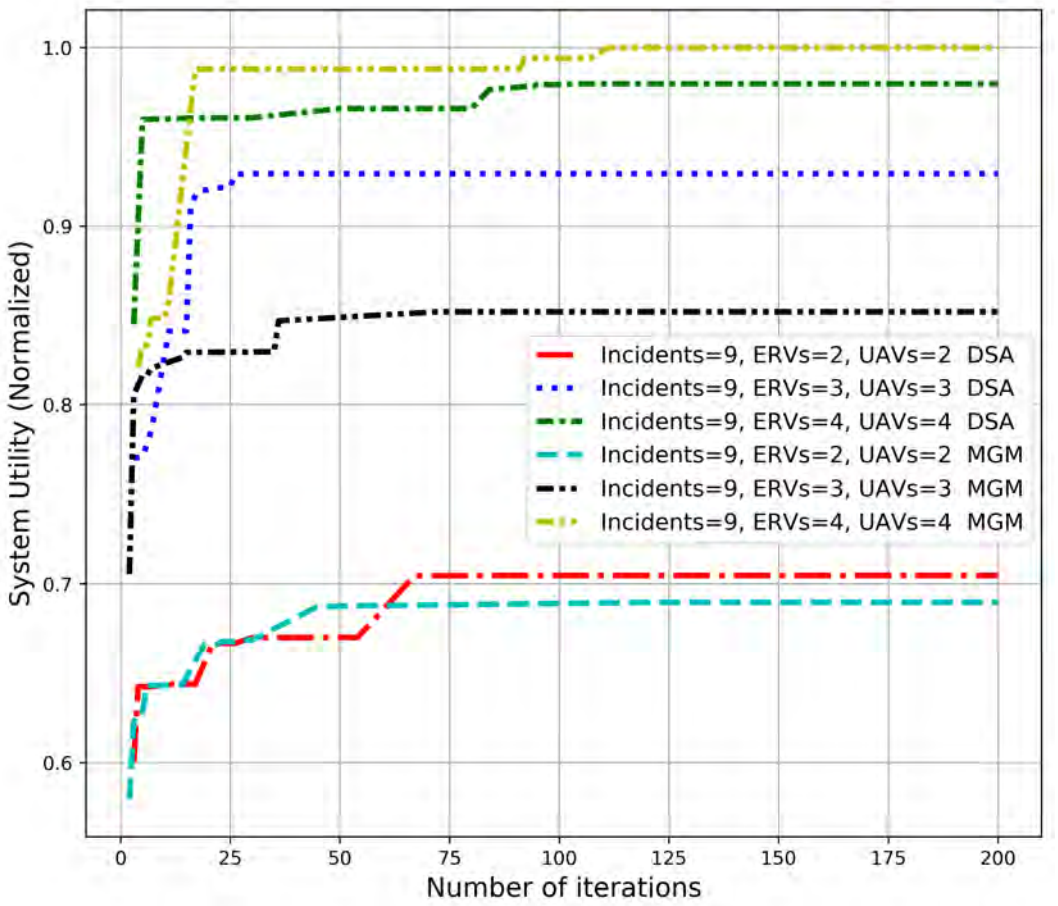

Figure 5: Convergence of MGM and DSA (p=0.5) for varying vehicle number with a fixed number of incident request.

The results in Figure 5 show the effects of varying the number of vehicles for a fixed number of incident requests. As expected, we observe that the system utility increases for increasing vehicle number for the same number of incident requests. Considering 9 requests, some occurring concurrently, the increase in the number of emergency vehicles means more resources are available

for those requests occurring concurrently and also for near-future requests. In general, we observe that the exploration heuristic of DSA leads to a better solution, as seen in DSA solutions for the cases of 2 and 3 vehicles (ERVs and UAVs).

Table 2: Performance of the DCOP Strategy and Proposed P-DRONETIM Model

Emerg. Req. Loc.		DCOP Dispatch loc. (**resp. time (min)**)				P-DRONETIM Dispatch loc. (**resp. time (min)**)			
Time		ERV1	ERV2	UAV1	UAV2	ERV1	ERV2	UAV1	UAV2
0	˘	4	8	8	9	4	8	8	9
1	2	2 (**16.8**)	8	2	9	2 (**16.8**)	5	2	5
2	1	1 (**11.4**)	8	1	9	1 (**11.4**)	4	1	5
3	4	1	4 (**3.6**)	4	9	1	4 (**0**)	4	2
4	3	3 (**13.2**)	4	3	9	3 (**13.2**)	1	3	1
5	9	3	9 (**17.4**)	3	9	9 (**17.7**)	7	9	7

To further assess the robustness of the model and test its suitability, we conduct a Monte Carlo simulation with 10 scenarios of randomly sampled vehicle number, number of incident requests, incident severity, and incident locations.

The results of the Monte Carlo simulation are shown in Figure 6. Implementing the exploration heuristic (DSA) resulted in an improved vehicle assignment, as seen with the increase in total utility compared to just the highly exploitative solution approach (MGM). Our initial assessment of varying the probability threshold in DSA does not show the apparent effects and will require further assessment.

Table 2 compares the DCOP strategy and the proposed P-DRONETIM. DCOP strategy makes inde-

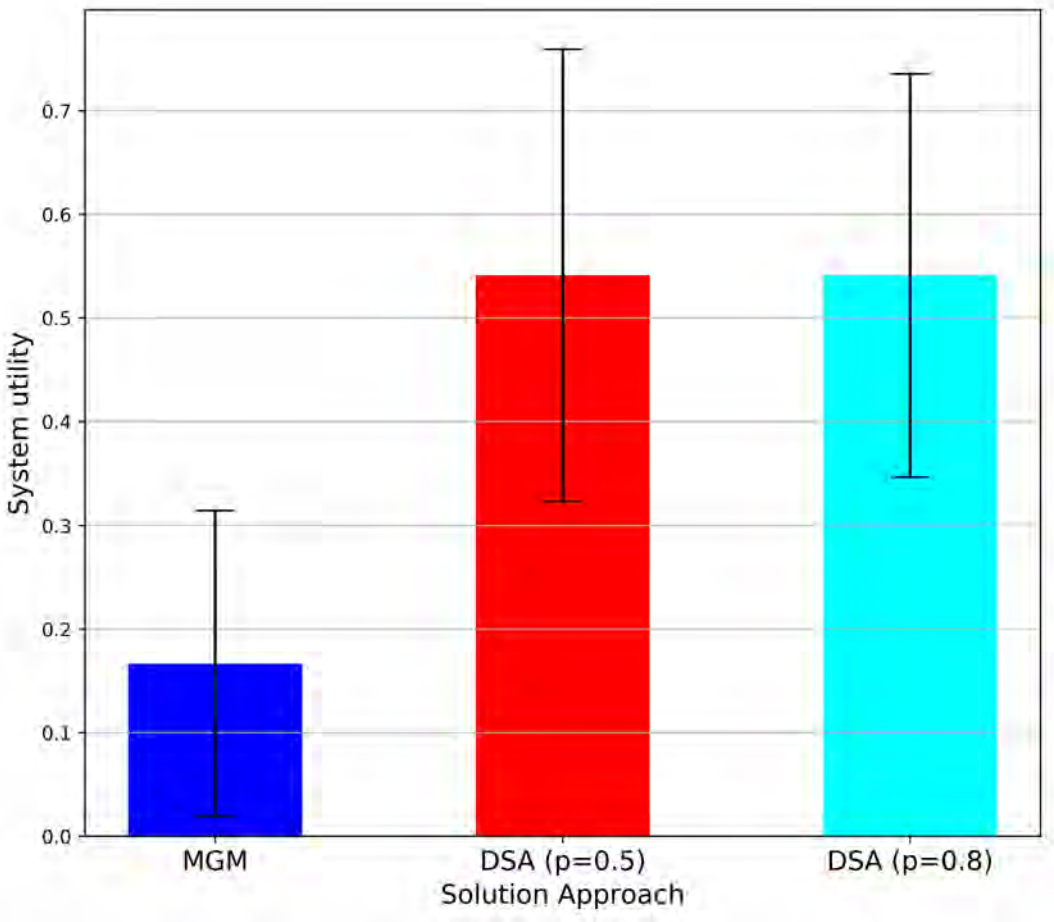

Figure 6: Results of Monte Carlo Simulation for MGM and DSA

pendent single-period decisions without considering future time stages. The illustration represents a scenario of five incident requests at different times with no concurrent emergencies. Incidents at locations 2, 1, 3, and 9 are minor crashes, and the incident at location 4 is a major crash. The estimates of the response time for the DCOP strategy ranges between 3.6 min and 17.4 min, with a total response time of 62.4 min. ERV1 is dispatched to incident requests at locations 2, 1, and 3, and ERV2 to incident requests at locations 4 and 9. In contrast to the DCOP strategy, the P-DRONETIM dispatched ERV1 to incident requests at locations 2, 1, 3, and 9, while ERV2 is optimally relocated to location 4 in anticipation of a near-future incident. This insight resulted in a 0 min response time for the incident request at location 4. The total response time for our model's strategy is estimated as 59.1 min, representing a 5.28% improvement in overall response time compared to the DCOP strategy. In the UAV plan, we observe high reliability to minimize assignment to locations with overlapping observation regions. We also observe that the DCOP strategy will assign UAV1 to the

incident requests 2, 1, 4, and 3 while UAV2 is assigned to incident request 9.

8 Conclusions

In this work, the use of P-DRONETIM provides a roadmap for practical resource allocation for highway incident management, fully integrating and utilizing the benefits of UAVs. The proposed framework implemented with MGM and further improved with an exploration heuristic presents better performance than the DCOP Strategy. Our model actively relocates emergency vehicles to anticipate future incidents to improve the overall response time to incident requests. Aside from UAVs' assignment to incident locations, the UAVs provide enhanced coverage of the transportation network by reducing location assignments that result in overlapping observations.

In future research, we intend to develop a two-level decision process for UAVs. The upper level is the location decision, determined from P-DRONETIM, while the lower level is the routing decision. The routing decision can be modeled to maximize the reduction in entropy (Folsom et al., 2021; Darko et al., 2020) for observed traffic parameters such as link travel time, shockwave parameters, and discharge rate resulting from an incident while en-route to an assigned location. While this study considered only primary incidents, occurring concurrently or in a sequence, when primary incidents occur in a sequence of time intervals, the likelihoods of secondary incidents caused by each primary incident are accumulated (Park et al., 2018; Park and Haghani, 2016b). The conditional probability of a secondary incident in the future depends jointly on the primary and secondary incidents that have occurred during past and present time stages. Additionally, past uncleared pending incidents continue to impact current and future incidents in the everyday highway incident scenarios. The mutual dependency between the states in different time stages should be considered in future studies.

PART TWO: SECONDARY CRASH ANALYSIS

Executive Summary

Traffic incidents can create major non-recurring congestion and have the potential to be fatal. Traffic Engineers and researchers have worked vigorously to reduce and prevent traffic crashes and make roadways safer. Secondary crashes are collisions that have taken place inside of incident scene or within the queue, influenced by the already occurred primary incident. Secondary crash occurrences are less frequent than primary incidents, however, the incident management without considering a potential secondary crash can cause a worst-case scenario to both emergency vehicles and travelers. Although statistical models have been developed in the past to estimate the probability of secondary crashes, they do not consider time-series changes of the probability. A Markov chain, a stochastic model is used in this study to model randomly-occurring incidents in a sequence. It is different from previously developed semi-Markov models by considering incident duration as a first-order to estimate the secondary crash parameters in the second order. Based on author's previous models on incident duration prediction, this study develops a multivariate second-order Markov model to estimate the probability of a secondary crash based on various primary incidents. This analysis will determine and identify if the probability of a secondary crash is higher at a specific location or higher due to a specific type of primary incident. Findings from our analysis can aid in developing countermeasures such as allowing emergency operators to allocate more resources to clear primary incidents quicker, or better prepare for secondary crashes based on the predicted probability of additional incidents.

9 Introduction

Traffic crashes are largely responsible for causing congestion on roads, and the outcome can be deadly. In 2016, there were 37,461 traffic crash fatalities reported in the United States alone (Releases, 2016), which accounted for a 5.6 % increase in traffic crash fatalities than the previous year (Releases, 2016). These incidents have caused 25% of all traffic delays experienced by drivers (Owens et al., 2010). Traffic incidents can be described as debris, collisions, and disabled vehicles that have resulted in frequent disruption of traffic operations (Yang et al., 2014a). These incidents

can affect the risk of another car being involved in a secondary collision. Studies show that 1% of crashes are entirely or partially a result of a primary incident (Raub, 1997). In addition to the type of incidents mentioned previously, secondary crashes can result from other actions such as rubbernecking, and buildup of the queue (traffic congestion) (Raub, 1997).

The Federal Highway Administration (FHWA) defines a secondary crash as "The number of secondary crashes beginning with the time of detection of the primary incident where a collision occurs either a) within the incident scene or b) within the queue, including the opposite direction, resulting from the original incident." Xiong et al. (2014b) FHWA estimates that nearly 20% of all crashes are secondary crashes (b6). It is estimated that 18% of all fatalities happen on interstates, due to secondary crashes (b7). The likelihood of a secondary crash will increase by 2.8% for each minute that a primary crash remains a hazard b8. With vehicle crashes costing the United States $242 billion dollars, agencies and researchers are constantly looking for ways to reduce and prevent traffic incidents (b9, 2015). Secondary incidents have been studied based on analyzing crash risk (Yang et al., 2014c,b), time period duration (Yang et al., 2014a,c; Goodall, 2017), incident duration (Khattak et al., 2009), real-time prediction (Park et al., 2017a; Park and Haghani, 2016c; Khattak et al., 2011), and crash severity (Xu et al., 2016). Compared to numerous studies on natural disasters, secondary crashes occur more often in everyday congestion. Even though secondary crash occurrences are less frequent than primary incidents, incident management without considering a potential secondary crash can cause a worst-case scenario to both emergency vehicles and travelers. Although statistical models have been developed in the past to estimate the probability of secondary crashes, time-series changes of the probability are not considered. A Markov chain, a stochastic model is used in this study to model randomly-occurring incidents in a sequence of events that have taken place previously. It is a useful model when modeling practical systems in transportation under uncertainty. By considering incident duration as a first-order to estimate the secondary crash parameters in the second-order, this study differentiates itself from a previously developed semi-Markov model (Ng et al., 2013). Based on the author's previous models on the prediction of incident duration and secondary likelihood (Park et al., 2017a; Park and Haghani, 2016c), this study develops a multivariate second-order Markov model to estimate the probability of a secondary crash based on various primary incidents, from Maryland Interstate 695 incident data.

For the remaining sections of this paper, we will discuss the previous studies regarding Markov

models and predicting secondary crashes; in the Methodology section, we will discuss using our high-order Markov model to predict secondary crashes based on different scenarios; followed by discussing the results and then conclude this work.

10 Literature Review

High order Markov models have been used for prediction in various topics: Spectrum usage (Li et al., 2010), sales demand (Ching et al., 2003), and DNA sequencing (Ching et al., 2004). Additionally, High-order Markov chains have had successful and widespread adoption in sensor and computer networks (Aceto et al., 2021; Rossi et al., 2015). Markov models have been used previously used to determine the time duration in-between a primary crash and secondary crash (Ng et al., 2013). However, the primary objective of this paper was to utilize high-order Markov models to conduct an analysis and calculate the probability of a secondary crash based on various primary incidents and locations. As a practical application, this second-order Markov model secondary crash prediction can be used for aiding emergency vehicle routing (Sayarshad and Chow, 2017; Djavadian and Chow, 2017; Chow and Nurumbetova, 2015; You et al., 2016).

Markov models have shown to be reliable at making predictions in the transportation field, more specifically in crash analysis. When the severity of crash data is reported, it is reported as discrete data. This has made crash injury severity observation a focus of many safety analyses (b7). Semi-Markov models have been used to model the time duration to the next primary and secondary incidents (Sayarshad and Chow, 2017). The authors used an original semi-Markov model (Janssen and Manca, 2006) to model primary incidents and extended the model to include secondary incidents. The results were able to show that if a freeway is heavily traveled and has a high-speed limit, it is more susceptible to incidents and it is harder to make an impact on the time to a secondary incident. Hidden Markov models, such as the one used in (Xiong et al., 2014a) are commonly used to determine unobserved heterogeneity across time periods. The goal was to expand transportation research by developing a Markov switching random parameters model and applying it to crash injury severity's. These findings will aid in a better understanding of how the effect of roadway and driver characteristics have on crash injuries. The states were split into two states (State I and State II) with three variables each: No injuries, Injury, and Fatality (y =1, y=2, y=3). The data used is the

Table 3: Model Category in Crash Detection

Author	Title	Paper Objective	Semi-Markov Model	Hidden Markov Model	High-Order Markov Model
M. Ng et. al	”Modeling the time to the next primary and secondary incident: A semi-Markov stochastic process approach”	Duration between primary and secondary crash	✓		
G. Aceto et. al	"Characterization and Prediction of Mobile-App Traffic Using Markov Modeling."	Traffic Prediction			✓
H. R. Sayarshad et. al	"Non-myopic relocation of idle mobility-on-demand vehicles as a dynamic location-allocation-queuing problem."	Emergency Vehicle Routing		✓	
Y. Xiong et. al	"The analysis of vehicle crash injury-severity data: A Markov switching approach with road-segment heterogeneity"	Crash injury analysis	✓		
H. Park et. al	"Modeling Effects of Forward Glance Durations on Latent Hazard Detection"	Hazard Detection		✓	
G. B. Singh et. al	"Crash Detection System Using Hidden Markov Models."	Vehicle Crash Detection		✓	
G. B. Singh et. al	"Comparison of Hidden Markov Models and Support Vector Machines for vehicle crash detection"	Vehicle Crash Detection		✓	
N. Pugh et. al	"High-Order Markov Model for Prediction of Secondary Crash Likelihood considering Incident Duration"	Secondary Incident Prediction			✓

Indiana police reported rural interstate single-vehicle crash from 1995 to 1999 (260 weeks). This data included factors such as roadway geometrics, pavement characteristics, driver characteristics,

and collisions. The model developed used a Markov Switching Random Parameters Ordered Probit (MSRPOP) model. The state was changed every week (St) to accommodate for the 260 weeks. From this study, factors such as international roughness index, rut depth, and average annual daily traffic were said to influence crash injury severity from the observed states. State 1 was said to be more related to a driving environment with a higher probability of an injury than state 2. Out of the analysis, 76 % of fatal crashes and 93 % of injury crashes had more than an 80% probability to occur in state one.

Other variations of a Markov model are when the actual state is not observable from the data. To estimate the hidden safety state, the author of this paper (Park et al., 2017b) developed a Hidden Markov Model (HMM). The estimated human intent as various types of secondary tasks to estimate the probability of hazard detection. Singh et al. (2004) developed a system for vehicle crash detection based on seven stages of left-right HMM. Left-Right HMM has shown to be successful when used in time series applications. The parameters and data generated for this research were both real and computer-aided engineering data. Crash pulses were used to train the HMM's. The pulses consisted of accelerometer measurements in a crash and the simulation of computer-aided engineering. The model was said to be 100% accurate and no cases of false positives or false negatives. The benefits of this model was: It was fast at detecting crashes ($\geq 6ms$), simple to implement since it only utilizes two sensors and an adaptable model that can be changed to use any vehicle line or additional sensors.

The same authors as the previous research (Singh et al., 2004) expanded their study by comparing HMM against Support Vector Machines (SVM) for vehicle crash detection (Singh and Song, 2010). HMM and SVM both perform well to optimizing their objective functions but performance can have different outcomes based on their assumptions. The data was for this project was acquired from a crash pulse library of a specific vehicle. The three groups of crash pulses were: vehicle crashes at 6 - 9 mph (low-speed crash), 12 - 25 mph (medium-speed crash), and high-speed crashes. The pulses were gathered from 27 crash experiments. The results were analyzed of a pulse rate from 4 – 8ms. For HMM, the average detection rates were: 99.4% (4ms), 99.3% (5ms), 100% (6ms). For SVM, average detection rates were: 99.4% (4ms), 99.8% (5ms), 99.9% (6ms), and 100% (7ms). Overall, this research showcased that HMMs can determine crash pulses from a non-crash pulse in 6ms and SVM can detect collisions in 7 ms. To summarize, although previous papers

have focused on modeling secondary crash risk using various factors, there have been no studies using a higher-order Markov model considering the impact of incident duration on secondary crash occurrences. We fill this gap by accomplishing the following contributions in this paper:

- This paper focuses on predicting whether a secondary crash will occur based on all incidents, the type of primary incident leading to a secondary crash, and exit locations.
- This paper explores secondary crash prediction using a high-order Markov approach to model and predict secondary crashes.
- This paper determines which starting sequences (stages) result in secondary crash identification.

Additionally, we will discuss the technical challenges faced in the Discussion section of this paper.

11 Methodology

We present a general Markov chain method utilized in the secondary crash prediction and extend it to higher-order Markov chain.

11.1 Markov Chains

A Markov chain is a random process in discrete time that is a sequence of a random variable. We can describe a Markov chain as follows: We have a set of states $X = \{X_1, X_2, X_3, \ldots, X_N\}$, N being the number of possible states. Markov chains have an initial state vector (N x 1 matrix) which is the probability distribution of starting at the N possible states. The initial state vector can be described as:

$$\Pi = \begin{bmatrix} \Pi_1 = P(x_1 = 1) \\ \Pi_2 = P(x_1 = 2) \\ \vdots \\ \Pi_N (q_1 = N) \end{bmatrix} \tag{18}$$

The stochastic property for the initial state distribution vector is:

$$\sum_{i=1}^{k} \Pi_i = 1 \tag{19}$$

$\Pi_i = 1$ is defined as:

$$\Pi_i = P\left(x_1 = i\right), 1 \leq i \leq N. \tag{20}$$

The process starts in state X_1, and will continue to move from one state to another. Every move to another state is considered to be a step. There is a probability associated with going from state to state which can be denoted as $P_{X_{ij}}$, i is the initial state and j is the next state. These probabilities are known as transition probabilities. A random process that has the Markov property if the conditional probability of future states depends on the present state, and not any events that preceded it. The conditional transition probabilities can be denoted by:

$$a_{X_{i-1}X_i} = \Pr\left(x_i | x_{i-1}\right) \tag{21}$$

and the probability of the next state of a first-order Markov model relationship can be denoted as :

$$\Pr\left(X_{t+1} = i_{t+1} \mid X_0 = i_0, X_1 = i_1, \ldots, X_t = l_t\right) = \Pr\left(X_{t+1} = i_{t+1} \mid X_t = i_t\right) \tag{22}$$

where x_t is the state of a categorical data sequence at time t. The transition probability matrix is a (I x J) matrix that can be denoted as:

$$A = \begin{bmatrix} a_{11} & a_{21} & \ldots & a_{1J} \\ a_{21} & a_{22} & \ldots & a_{2J} \\ \vdots & \vdots & \ddots & \vdots \\ a_{11} & a_{12} & \ldots & a_{IJ} \end{bmatrix} \tag{23}$$

Equations (1) – (6) describe the equations and properties of a first-order Markov process.

A high-order Markov model can be used to predict future states as well. A high-order Markov model will utilize more memory when making predictions. The next state will depend on the previous two or more states. For example, if you were trying to predict the next word in a sequence, it may be helpful to know the previous two words rather than just one previous word. In high-order

Markov models, the previous history can have predictive value and can be used when making a future prediction.

$$x_{r+1}^{(j)} = \sum_{k=1}^{s} \sum_{h=1}^{n} \lambda_{jk}^{h} P_{h}^{(jk)} x_{r-h+1}^{k}, j = 1, 2, \ldots, s, r = n-1, n, \ldots \tag{24}$$

where the initial probability distributions are $x_0^{(1)}$,
$x_0^{(2)}, \ldots, x_0^{(n)}$ and $\lambda_{j,k}^{(h)}$ satisfies

$$\sum_{k=1}^{S} \sum_{h=1}^{n} \lambda_{j,k}^{(h)} = 1, j = 1, 2, \ldots, s \tag{25}$$

$$\lambda_{j,k}^{(h)} \geq 0, 1 \leq j, k \leq s, 1 \leq h \leq \mathrm{n} \tag{26}$$

Equations (7) – (9) describe the equations and properties of a high-order Markov process.
When making predictions, the sequences of secondary incidents needs to be fit to a Markov model. We estimate our higher-order Markov model by solving the linear-quadratic programming problem:

$$\begin{aligned} \min \left\| \sum_{i=1}^{k} \boldsymbol{X} - \lambda_i Q_i \boldsymbol{X} \right\| \\ \mathbf{s.t.} \\ \sum_{i=1}^{k} \lambda_i = 1 \\ \lambda_i \geq 0 \end{aligned} \tag{27}$$

State distributions are given X, λ_i is lag parameter for lag i and Q_i is transition matrix. The heat map displays the transition probabilities for our fitted Markov model. After fitment of the high-order Markov model, a starting sequence is given and the next sequence can be predicted. The next sequence is predicted based on the transition probabilities of the fitted high-order Markov model. We estimate the probability distribution of the next sequence as:

$$X^{(t)} = B \cdot \sum_{i=1}^{k} \lambda_i Q_i X^{(t-i)} \tag{28}$$

where distribution of states are at time t, and is given as $X^{(t)}$. The transition matrix of lag i is given as Q_i, and λ_i specifies the lag parameter. B is the absorbing probability matrix.

11.2 High-Order Multivariate Markov Model Secondary Crash Application

In the previous section, we introduced the general Markov chain used to model and predict secondary crashes. The general Markov chain is then extended to a higher-order multivariate method. Our model is used to find the probability of a secondary crash given a primary incident. The 4 possible states are P, S, C, NO.

- P = primary incident
- S = secondary crash
- C= clearance of an incident
- NO = nothing happened (the state has not changed)

Each primary incident and the following states will be considered a sequence. There were a total of 39 incidents recorded. The 39 incidents were then grouped into 20 incident sequences. (One primary crash and one secondary crash per sequence). In our analysis, we have 3 different scenarios. The scenarios were:

- All the sequences were used to fit the Markov model.
- Various primary incident types (disabled vehicles, primary collision, and obstructions) were used to fit the model.
- Grouped exit incident locations along Interstate 695.

The assumptions are:

- Sequences were only modeled up to 60 minutes starting from the primary incident.
- Each stage time step was taken in 15 minutes intervals.
- When fitting the model, sequences were recorded until there were two clearances (both incidents were cleared).

- When modeling, because a primary incident clearance and a secondary crash could both occur within a 15-minute time interval, whichever event came first was recorded as the first stage. The next stage would be the following event.
- Each model scenario was given three starting sequences 1. (p) (c) 2. (p) (s), and 3. (p) (no) to determine the prediction of the next two stages (30 minutes).

The scenarios will be described in the Results section and a probability of the predicted sequence will be given.

Figure 7: Heat Map for Transition Probabilities

For a visual representation of transition probabilities, a heat map (Figure 1) and Markov chain diagram (Figure 2) were created from the fitting of our model. The figures are the actual heat map and Markov model for the “All Incidents” scenario. The heat map can be explained as the "greener" the block the higher the associated probability. The Y-axis (From) is the beginning state and the X-axis (TO) is the ending state. For example, let us look at the (p) row on the heat map. From p to c (primary incident to a clearance) the probability is 20%. From (p) to (s) (primary incident to

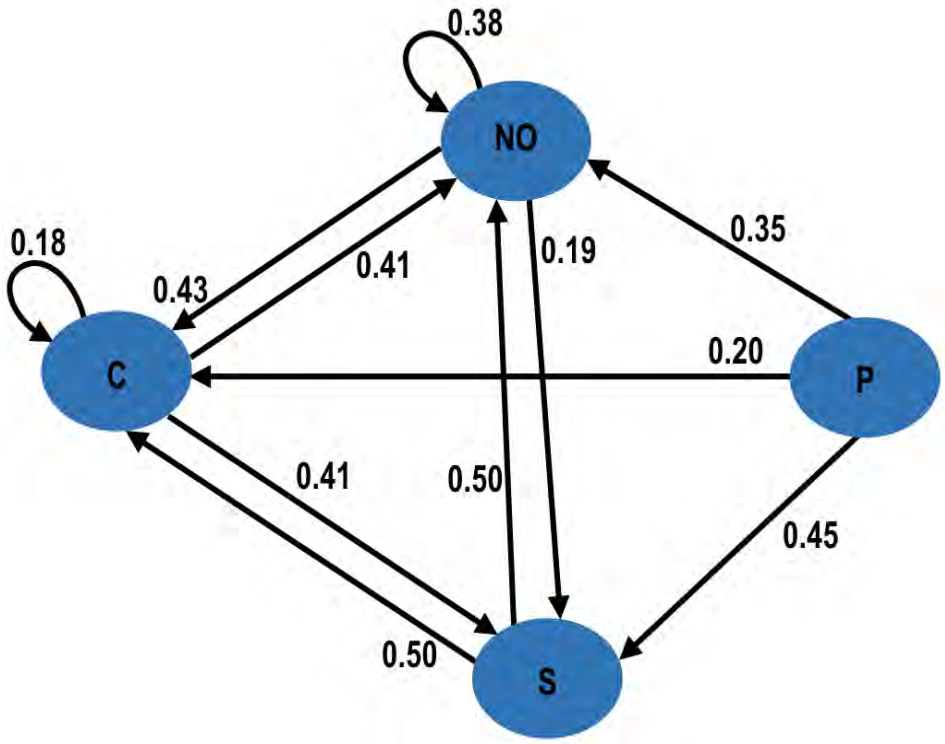

Figure 8: Markov Chain Diagram for Transition Probabilities

secondary crash) there is a 45% probability. From (p) to (no) (primary incident to nothing happens) there is a 35% chance nothing will happen (the state will stay the same). When starting from a secondary crash, there is a 50% chance that nothing will happen and a 50% chance a clearance will occur within the next 15 minutes.

11.3 Data Description

The incident data was provided by The Regional Integrated Transportation Information System (RITIS) to find the probability of a secondary crash given a primary incident on Interstate 695 (I-695) in Maryland. The RITIS dataset provides valuable information such as incident location, time, type of incident, and incident duration. In Figure 3, the total number of incidents that occurred on Interstate 695 occurred during June 2018. For our analysis, we used incidents that occurred within the 30-mile section from exit 10 to exit 35, which is highlighted in red. Out of all the incidents shown, we classified 20 incidents as being secondary crashes. Table 1 displays the incident data statistics such as location, incident type, and incident duration. A previously developed secondary crash identification method (Park et al., 2017b) (Figure 4) was utilized for all the above incidents.

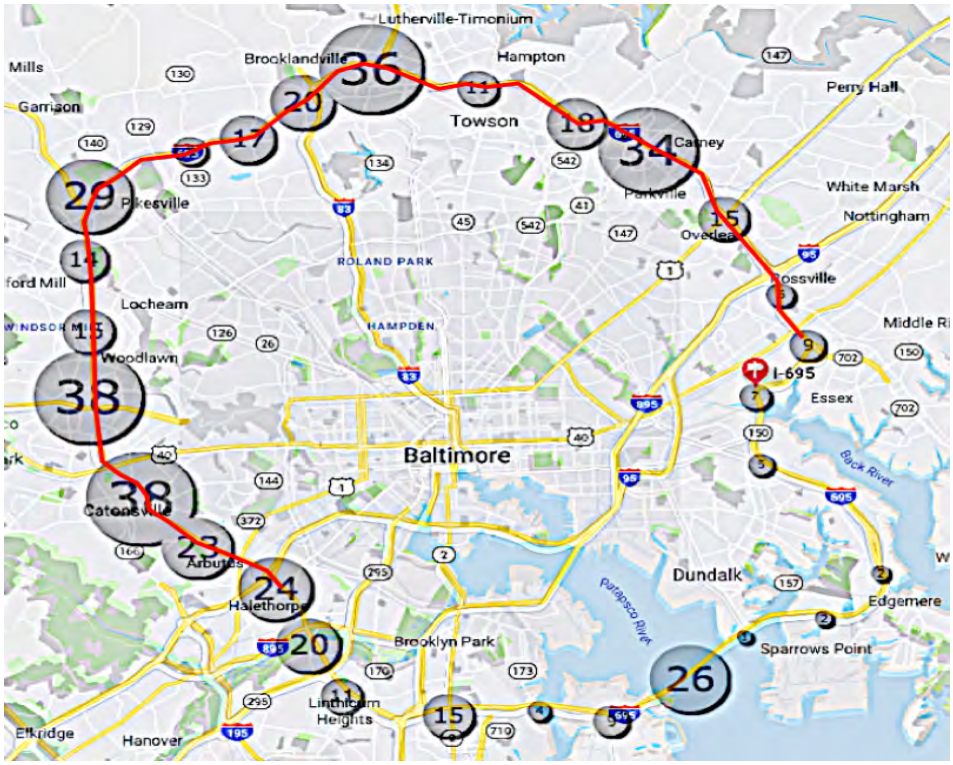

Figure 9: Secondary Incident Locations: I-695.

12 Results

To determine how much the model can be trusted, we tested the model for its prediction accuracy shown in Table 2. To determine the accuracy, we found the accuracy for each scenario separately and then averaged the final accuracies to determine the overall prediction accuracy of the model. When testing, a sequence was removed from each scenario at random. The remaining sequences were used to fit the model. After completing the fitting, the model was giving the starting sequence of the removed sequence to make its prediction of the next two stages. The results indicated that in 6/9 of the scenarios the model predicted one of the stages correctly and received an accuracy of 50%. In 3/9 of the scenarios, the model predicted the next two stages correctly and received an accuracy of 100%. There were no cases where the model did not predict any of the next two stages correctly. The overall prediction accuracy of the model is 66.7%.

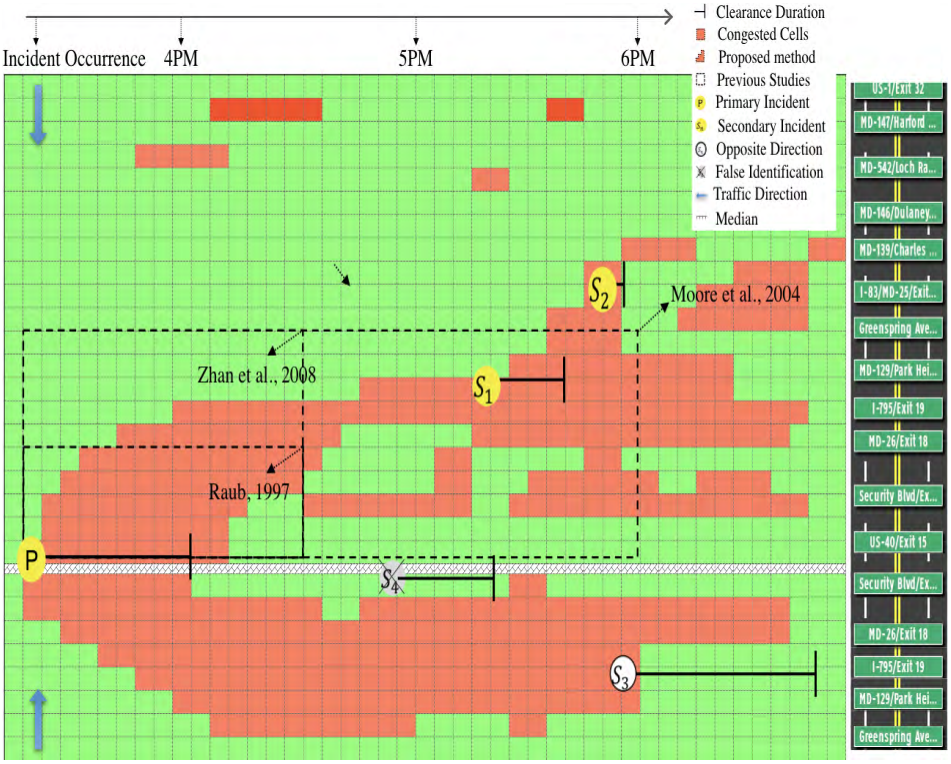

Figure 10: Secondary Crash Identification

As previously mentioned, different scenarios will be used to determine the probability of a secondary crash. Table 1 shows the scenarios indicating that a secondary crash was predicted. The scenarios are as follows: All Events, Primary Incident, and Exit Number Location. The first scenario All Events (Table 3) uses all 20 grouped incident sequences to fit the model. The model was given the three starting sequences stated previously. The results indicated that after a primary incident and a clearance, the model predicted there will be a secondary incident and a clearance within the next 30 minutes. Additionally, when a primary incident and secondary incident occur, shortly after clearance of one of the incidents will take place followed by another secondary crash. Both of these scenarios had a 12.9% probability.

The second scenario was the primary incident secondary crash prediction (Table 4). Since secondary crashes can be caused by different types of primary incidents, we decided to separate the sequences by the type of primary incident that leads to the secondary crash. It is interesting to note that there was only one scenario where the model predicted a secondary crash. The model predicted a secondary crash when the primary incident was an obstruction on the highway. The

Table 4: Secondary Incidents Statistics Part I

Incident Type	Primary or Secondary Incident	Location	Incident Duration
Collision	Primary	Exit 32	23 minutes
Collision	Secondary	Exit 29	38 minutes
Collision	Primary	Exit 31	27 minutes
Collision	Secondary	Exit 30	2 minutes
Collision	Primary	Exit 24	8 minutes
Collision	Secondary	Exit 24	31 minutes
Obstruction	Primary	Exit 18	42 minutes
Collision	Secondary	Exit 18	3 minutes
Collision	Primary	Exit 11	43 minutes
Collision	Secondary	Exit 11	2 minutes
Disable Vehicle	Primary	Exit 10	2 minutes
Collision	Secondary	Exit 10	32 minutes
Disabled Vehicle	Primary	Exit 32A	3 minutes
Collision	Secondary	Exit 32A	11 minutes
Disabled Vehicle	Primary	Exit 23A	1 hr. 27 min.
Collision	Secondary	Exit 23A	25 minutes
Collision	Primary	Exit 23A	25 minutes
Collision	Secondary	Exit 22	39 minutes
Disabled Vehicle	Primary	Exit 21	1 minute
Collision	Secondary	Exit 21	34 minutes
Obstruction	Primary	Exit 30A	1 hr. 36 min.
Collision	Secondary	Exit 30A	3 hr. 42 min.
Disabled Vehicles	Primary	Exit 29	33 minutes
Collision	Secondary	Exit 30	41 minutes
Disabled Vehicle	Primary	Exit 16	1 minute
Collision	Secondary	Exit 16	28 minutes
Disabled Vehicle	Primary	Exit 17	52 minute
Collision	Secondary	Exit 17	28 minutes
Collision	Primary	Exit 19	1 hr. 2 min.
Collision	Secondary	Exit 19	1 minute
Disabled Vehicle	Primary	Exit 18	31 minutes
Collision	Secondary	Exit 18	1 hr. 4 min.
Disabled Vehicle	Primary	Exit 31A	1 minute
Collision	Secondary	Exit 31A	34 minutes
Disabled Vehicle	Primary	Exit 26A	10 minutes
Collision	Secondary	Exit 25	16 minutes
Obstruction	Primary	Exit 28	19 minutes
Collision	Secondary	Exit 29B	34 minutes
Collision	Primary	Exit 12	22 minutes
Collision	Secondary	Exit 12	11 minutes

Table 5: Model Prediction Accuracy

Scenario	Prediction Accuracy
All Incidents	50%
Collision	50 %
Disable Vehicles	50 %
Obstruction	100%
Exits 10 - 15	100%
Exits 15 - 20	50 %
Exits 20 - 25	50 %
Exits 25 - 30	100 %

Table 6: All Incidents Event Secondary Crash Prediction (Scenario I)

Scenario	Starting Sequence	Next Predicted Stages (n=2)	Probability
*All Events	(p) (c)	(s)(c)	0.129
*All Events	(p) (s)	(c) (s)	0.129
All Events	(p) (no)	(c) (no)	0.110

starting sequence given for that scenario was a primary incident followed by a clearance of the incident. The associated probability was 60%.

Table 7: Primary Incident and Secondary Crash Prediction (Scenario II)

Primary Incident Type	Starting Sequence	Next Predicted Stages (n=2)	Probability
*Obstruction	(p) (c)	(s)(no)	0.600
Obstruction	(p) (s)	(no) (no)	0.227
Obstruction	(p) (no)	(no) (no)	0.110
Disabled Vehicles	(p) (c)	(no) (c)	0.205
Disabled Vehicles	(p) (s)	(no) (c)	0.220
Disabled Vehicles	(p) (no)	(c) (no)	0.205
Collision	(p) (c)	(c) (c)	0.148
Collision	(p) (s)	(c) (c)	0.247
Collision	(p) (no)	(no) (no)	0.148

For the final scenario (Table 5) we split the incidents based on the location that they occurred. The exit numbers were separated into groups of 5. The exits where the incidents occurred were from exits 10 – 35. This was to determine whether there was a location that was more susceptible to secondary crashes. From our results exit 15 - 20, there were two scenarios where secondary incidents were predicted. The starting sequences for those two scenarios were: (p) (c) and (p) (no). Also, the prediction made on one of the scenarios for exit 15 – 20 was the highest for this scenario

Table 8: Exit Number Group Secondary Crash Prediction (Scenario III)

Exit Numbers	Starting Sequence	Next Predicted Stages (n=2)	Probability
*Exits 10 - 15	(p) (c)	(s)(c)	0.213
Exits 10 - 15	(p) (s)	(c) (c)	0.213
Exits 10 - 15	(p) (no)	(no) (no)	0.284
*Exits 15 - 20	(p) (c)	(s) (no)	0.380
Exits 15 - 20	(p) (s)	(no) (c)	0.319
*Exits 15 - 20	(p) (no)	(c) (s)	0.172
Exits 20 - 25	(p) (c)	(no) (c)	0.295
Exits 20 - 25	(p) (s)	(c) (no)	0.330
Exits 20 - 25	(p) (no)	(c) (no)	0.295
*Exits 25 - 30	(p) (c)	(s) (no)	0.147
Exits 25 - 30	(p) (s)	(c) (no)	0.147
Exits 25 - 30	(p) (no)	(c) (no)	0.147
*Exits 30 - 35	(p) (c)	(s) (no)	0.160
Exits 30 - 35	(p) (s)	(no) (no)	0.134
Exits 30 - 35	(p) (no)	(no) (no)	0.170

group at 38.0%. For every exit group except exits 20 – 25, when the starting sequence was (p) (c) there was a secondary incident predicted. The probabilities for exit 10 – 15 (21.3%), 15 -20 (38.0%), 25 – 30 (14.7%), and 30 - 35 (16.0%). The next predicted stages for exits 15 – 20, 25 – 30, and 30 - 35 all predicted the same "next predicted stages" as (s) (no). For exit 10 – 15, the next stage predicted stage was (s) (c). For exit 15 - 20, the next predicted stage was (c) (s). Our results also indicated that after a primary incident and clearance a secondary crash was predicted.

Out of all the examples tested, there were 8 instances where secondary crashes were predicted. We wanted to determine which starting sequence was the most frequent in predicting a secondary incident. The results for this question are shown in Figure 3. Out of the 8 instances, the starting sequence (p) (c) accounted for 75 % (6) of the instances where secondary incidents were predicted. Both of the sequences (p) (no) and (p) (s) accounted for 12.5 % (1) of the secondary incidents being predicted. This shows that typically when a primary crash is followed by a clearance, a secondary crash is more predicted to occur within the next two stages (30 minutes) than compared to the other starting sequences.

We have identified some research papers that focus on traffic crash prediction including secondary incident prediction. The research papers compared in the table above use various different modeling approaches such as: Bayesian Random Effect Logit Model, Support Vector Machine (SVM)

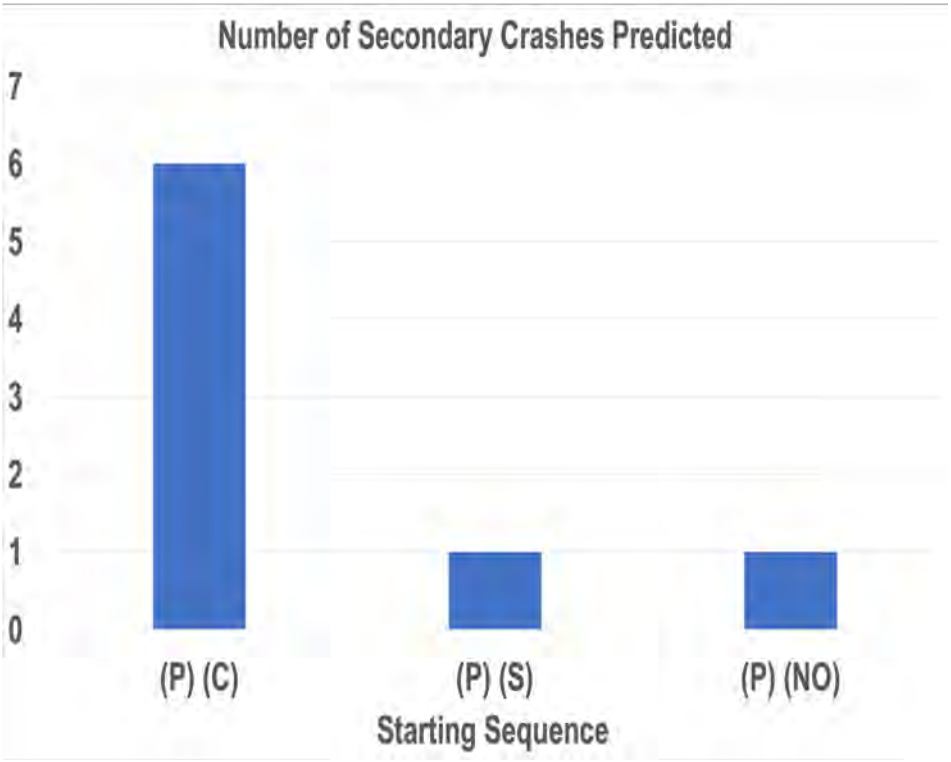

Figure 11: Number of secondary crashes predicted.

and Binary Logistic Regression. The accuracy rates range from 60.0% to 76.32%. Out of the models presented, our model (66.7%) has a higher prediction accuracy than three of the modeling approaches, including the model used to predict secondary incidents. Our model shows to preform similar or better to current modeling approaches for crash prediction. We believe our model accuracy will also improve even more with the use of additional data.

Table 9: Performance of existing models compared to proposed model

Author	Title	Model	Accuracy
C. Xu et. al	Real-time estimation of secondary crash likelihood on freeways using high-resolution loop detector data	Bayesian Random Effect Logit Model	66.0%
J. You. et. al	Real-time freeway crash prediction model by using single ultrasonic detector lane-level data	Binary Logistic Regression	61.0%
M. Hossain et. al	A Bayesian network based framework for real-time crash prediction on the basic freeway segments of urban expressways	Baysian Beleif Method	66.0%
Ahmed et. al	Bayesian updating approach for real-time safety evaluation with automatic vehicle identification data.	Bayesian Update Model	72.0%
J. You. et. al.	Real-time crash prediction on freeways using data mining and emerging techniques	Support Vector Machine (SVM)	76.32% (test dataset)
M. Wu. et. al.	A Bayesian Network Model for Real-time Crash Prediction Based on Selected Variables by Random Forest	Bayesian Network-Random Forest (BN-RF)	70.46%
Pugh et. al	High-Order Markov Model for Prediction of Secondary Crash Likelihood considering Incident Duration	High-Order Markov Model	66.7%

13 Discussion

13.1 Technical Challenges

There were two primary technical challenges that we faced in our research. The first challenge was selecting a relevant incident duration time. Due to the implementation of the ”Nothing happens” states, one could technically make a prediction from a starting sequence of two "Nothing happens" states. This could be a little confusing for the model when making a prediction. The model would be making a prediction using sequences were no event (primary incident) has occurred. For this reason, that is why we chose short sequences (only 1 hour total and 15 minute increments). Additionally, the starting sequences are chosen strategically as they only have at most one ”NO” state in the model fitment process. Considering we are only predicting the next 30 minutes, the only time where two "Nothing happens" states would occur would be for starting sequence 3: (p)(no), or if that was the predicted next two states. For the latter example, there is a possibility that two "Nothing happens" states can occur. However, because the sequence starts with the primary incident, the

model will know that an event (primary incident) has already occurred.

The second technical challenge was access to limited data. Due to the fact that our data was limited in number of secondary incidents occurring, there was little data to fit the model. However, we believe this modeling approach is promising and plan to further investigate these prediction matters in future works where we will have more data available.

13.2 Computational Complexity

The hardware used to support this work was a 2018 Apple Macbook Pro 2.9 GHz 6-Core Intel Core i9, with 32 GB of RAM. Considering our model is relatively light and the sequences used to fit the model are all short; the run-time complexity of our model is quite efficient. The average run time of our model using 20 secondary incident sequences was 0.0474 seconds. If we doubled our secondary incident sequences by 40 sequences the average run-time would be 0.0533 seconds. If we increased the fit of the model to 100 secondary incident sequences the average run-time would be 0.1176 seconds.

13.3 Future Studies

Crashes and traffic incidents are known for the potential of causing serious crashes and heavy congestion. Even though numerous projects have worked on natural disasters regarding secondary crashes, secondary crashes occur more often in everyday congestion scenarios. Previous researchers have focused on various aspects of modeling, predicting, and preventing secondary incidents. These findings have resulted in numerous amounts of valuable information regarding how to handle secondary crashes that will need to be investigated. We have added to this conversation by analyzing secondary crashes regarding the primary incident type, and incident exit location using a high-order Markov model. The second-order Markov model had an overall prediction accuracy of 66.7 %. Our findings indicate when an obstruction is a primary incident there is a high probability that a secondary crash will occur within the next 30 minutes after the primary obstruction incident and its clearance. Also, in most of our tests, when a primary crash and a clearance take place there

was a secondary incident predicted within the next 30 minutes.

For future studies, we would like to obtain data where more secondary crashes are present for better modeling of secondary incidents. As well, we would like to include more historical data to better fit models for making secondary crash predictions. The question of is more history needed when giving starting sequences or should more stages be predicted when predicting secondary crashes will need to be investigated. Additionally, we plan to re-investigate the run-time complexity using these longer sequences and larger dataset. We would also like to further investigate the use of second-order Markov models in assisting emergency vehicles in managing the disbursement of emergency vehicles to clear the primary incident and prevent secondary crashes.

REFERENCES

Next-generation tim: Integrating technology, data, and training. URL https://www.fhwa.dot.gov/innovation/everydaycounts/edc_6/nextgen_tim.cfm.

Secondary crashes. URL http://nchrptimpm.timnetwork.org/?page_id=23.

Road crash statistics. URL http://asirt.org/initiatives/informing-road-users/road-safety-facts.

Traffic incident management (tim) performance measurement: On the road to success. URL http://ops.fhwa.dot.gov/publications/fhwahop10009/tim_fsi.html.

Fhwa fsp handbook. URL https://ops.fhwa.dot.gov/publications/fhwahop08031/fsp4_0.htm.

Nhtsa study shows economic and societal impacts of crashes, 2015.

Giuseppe Aceto, Giampaolo Bovenzi, Domenico Ciuonzo, Antonio Montieri, Valerio Persico, and Antonio Pescapé. Characterization and prediction of mobile-app traffic using markov modeling. *IEEE Transactions on Network and Service Management*, 18(1):907–925, 2021.

Brian Cheung, Samuel Davey, and Douglas Gray. Comparison of the pmht path planning algorithm with the genetic algorithm for multiple platforms. In *2010 13th International Conference on Information Fusion*, pages 1–8. IEEE, 2010.

Wai Ki Ching, Eric S Fung, and Michael K Ng. Higher-order markov chain models for categorical data sequences. *Naval Research Logistics (NRL)*, 51(4):557–574, 2004.

WK Ching, ES Fung, and MK Ng. A higher-order markov model for the newsboy's problem. *Journal of the Operational Research Society*, 54(3):291–298, 2003.

Joseph YJ Chow and Adel E Nurumbetova. A multi-day activity-based inventory routing model with space–time–needs constraints. *Transportmetrica A: Transport Science*, 11(3):243–269, 2015.

Justice Darko, Larkin Folsom, Hyoshin Park, Masashi Minamide, Masahiro Ono, and Hui Su. A sampling-based path planning algorithm for improving observations in tropical cyclones. *Earth and Space Science Open Archive*, page 17, 2020. doi: 10.1002/essoar.10504807.1. URL `https://doi.org/10.1002/essoar.10504807.1`.

Justice Darko, Folsom Larkin, Niharika Deshpande, and Hyoshin Park. Distributed constraint optimization problem for coordinated response of unmanned aerial vehicles and ground vehicles. In *2021 55th Annual Conference on Information Sciences and Systems (CISS)*, 2021a.

Justice Darko, Folsom Larkin, and Hyoshin Park. Dynamic routing of unmanned-aerial and emergency team incident management (dronetim). In *2021 Proceedings of the TSL Second Triennial Conference*. Transportation Science and Logistics Society, 2021b.

Shadi Djavadian and Joseph YJ Chow. An agent-based day-to-day adjustment process for modeling 'mobility as a service'with a two-sided flexible transport market. *Transportation research part B: methodological*, 104:36–57, 2017.

Alessandro Farinelli, Alex Rogers, and Nick R Jennings. Agent-based decentralised coordination for sensor networks using the max-sum algorithm. *Autonomous agents and multi-agent systems*, 28(3):337–380, 2014.

PB Farradyne. Traffic incident management handbook. *Prepared for Federal Highway Administration, Office of Travel Management*, 2000.

Larkin Folsom, M. Ono, and Hyoshin Park K. Otsu. Scalable information-theoretic path planning for a rover-helicopter team in uncertain environments. *International Journal of Advanced Robotic Systems*, 2021.

Noah J Goodall. Probability of secondary crash occurrence on freeways with the use of private-sector speed data. *Transportation research record*, 2635(1):11–18, 2017.

Manish Jain, Matthew Taylor, Milind Tambe, and Makoto Yokoo. Dcops meet the real world: Exploring unknown reward matrices with applications to mobile sensor networks. *practice*, 20 (15):19, 2009.

Jacques Janssen and Raimondo Manca. *Applied semi-Markov processes*. Springer Science & Business Media, 2006.

Asad Khattak, Xin Wang, and Hongbing Zhang. Are incident durations and secondary incidents interdependent? *Transportation Research Record*, 2099(1):39–49, 2009.

Asad J Khattak, Xin Wang, Hongbing Zhang, Mecit Cetin, et al. Primary and secondary incident management: Predicting durations in real time. Technical report, Virginia Center for Transportation Innovation and Research, 2011.

Thomas Léauté and Boi Faltings. Distributed constraint optimization under stochastic uncertainty. In *Proceedings of the AAAI Conference on Artificial Intelligence*, volume 25, 2011.

Yang Li, Yu-ning Dong, Hui Zhang, Hai-tao Zhao, Hai-xian Shi, and Xin-xing Zhao. Spectrum usage prediction based on high-order markov model for cognitive radio networks. In *2010 10th IEEE International Conference on Computer and Information Technology*, pages 2784–2788. IEEE, 2010.

Rajiv T Maheswaran, Jonathan P Pearce, and Milind Tambe. A family of graphical-game-based algorithms for distributed constraint optimization problems. In *Coordination of large-scale multiagent systems*, pages 127–146. Springer, 2006.

Roger Mailler. Comparing two approaches to dynamic, distributed constraint satisfaction. In *Proceedings of the fourth international joint conference on Autonomous agents and multiagent systems*, pages 1049–1056, 2005.

Pragnesh Jay Modi. *Distributed constraint optimization for multiagent systems*. PhD thesis, University of Southern California, 2003.

Pragnesh Jay Modi, Wei-Min Shen, Milind Tambe, and Makoto Yokoo. Adopt: Asynchronous distributed constraint optimization with quality guarantees. *Artificial Intelligence*, 161(1-2): 149–180, 2005a.

Pragnesh Jay Modi, Wei-Min Shen, Milind Tambe, and Makoto Yokoo. Adopt: Asynchronous distributed constraint optimization with quality guarantees. *Artificial Intelligence*, 161(1-2): 149–180, 2005b.

ManWo Ng, Asad Khattak, and Wayne K Talley. Modeling the time to the next primary and secondary incident: A semi-markov stochastic process approach. *Transportation Research Part B: Methodological*, 58:44–57, 2013.

Nicholas Owens, April Armstrong, Paul Sullivan, Carol Mitchell, Diane Newton, Rebecca Brewster, and Todd Trego. Traffic incident management handbook. Technical report, 2010.

Hyoshin Park and Ali Haghani. Stochastic capacity adjustment considering secondary incidents. *IEEE Transactions on Intelligent Transportation Systems*, 17(10):2843–2853, 2016a.

Hyoshin Park and Ali Haghani. Real-time prediction of secondary incident occurrences using vehicle probe data. *Transportation Research Part C: Emerging Technologies*, 70:69–85, 2016b.

Hyoshin Park and Ali Haghani. Real-time prediction of secondary incident occurrences using vehicle probe data. *Transportation Research Part C: Emerging Technologies*, 70:69–85, 2016c.

Hyoshin Park, Ali Shafahi, and Ali Haghani. A stochastic emergency response location model considering secondary incidents on freeways. *IEEE Transactions on Intelligent Transportation Systems*, 17(9):2528–2540, 2016.

Hyoshin Park, Song Gao, and Ali Haghani. Sequential interpretation and prediction of secondary incident probability in real time. Technical report, 2017a.

Hyoshin Park, Song Gao, and Siby Samuel. Modeling effects of forward glance durations on latent hazard detection. *Transportation research record*, 2663(1):90–98, 2017b.

Hyoshin Park, Ali Haghani, Siby Samuel, and Michael A Knodler. Real-time prediction and avoidance of secondary crashes under unexpected traffic congestion. *Accident Analysis & Prevention*, 112:39–49, 2018.

Hyoshin Park, Deion Waddell, and Ali Haghani. Online optimization with look-ahead for freeway emergency vehicle dispatching considering availability. *Transportation research part C: emerging technologies*, 109:95–116, 2019.

Jonathan P Pearce and Milind Tambe. Quality guarantees on k-optimal solutions for distributed constraint optimization problems. In *IJCAI*, pages 1446–1451, 2007.

Richard A Raub. Occurrence of secondary crashes on urban arterial roadways. *Transportation Research Record*, 1581(1):53–58, 1997.

USDOT Releases. Fatal traffic crash data. *Article (CrossRef Link)*, 2016.

Pierluigi Salvo Rossi, Domenico Ciuonzo, and Torbjörn Ekman. Hmm-based decision fusion in wireless sensor networks with noncoherent multiple access. *IEEE Communications Letters*, 19 (5):871–874, 2015.

Hamid R Sayarshad and Joseph YJ Chow. Non-myopic relocation of idle mobility-on-demand vehicles as a dynamic location-allocation-queueing problem. *Transportation Research Part E: Logistics and Transportation Review*, 106:60–77, 2017.

Thomas Schiex, Hélene Fargier, Gerard Verfaillie, et al. Valued constraint satisfaction problems: Hard and easy problems. *IJCAI (1)*, 95:631–639, 1995.

Gautam B Singh and Haiping Song. Comparison of hidden markov models and support vector machines for vehicle crash detection. In *2010 International Conference on Methods and Models in Computer Science (ICM2CS-2010)*, pages 1–6. IEEE, 2010.

Gautam B Singh, Haiping Song, and Clifford C Chou. Crash detection system using hidden markov models. Technical report, SAE Technical Paper, 2004.

Gerald Steinbauer and Alexander Kleiner. Towards csp-based mission dispatching in c2/c4i systems. In *2012 IEEE International Symposium on Safety, Security, and Rescue Robotics (SSRR)*, pages 1–6. IEEE, 2012.

Gerard Tel. *Introduction to distributed algorithms*. Cambridge university press, 2000.

Yingge Xiong, Justin L Tobias, and Fred L Mannering. The analysis of vehicle crash injury-severity data: A markov switching approach with road-segment heterogeneity. *Transportation research part B: methodological*, 67:109–128, 2014a.

Yingge Xiong, Justin L Tobias, and Fred L Mannering. The analysis of vehicle crash injury-severity data: A markov switching approach with road-segment heterogeneity. *Transportation research part B: methodological*, 67:109–128, 2014b.

Chengcheng Xu, Pan Liu, Bo Yang, and Wei Wang. Real-time estimation of secondary crash likelihood on freeways using high-resolution loop detector data. *Transportation research part C: emerging technologies*, 71:406–418, 2016.

Hong Yang, Bekir Bartin, and Kaan Ozbay. Mining the characteristics of secondary crashes on highways. *Journal of transportation engineering*, 140(4):04013024, 2014a.

Hong Yang, Kaan Ozbay, Ender Faruk Morgui, Bekir Bartin, and Kun Xie. Development of online scalable approach for identifying secondary crashes. *Transportation Research Record*, 2470(1): 24–33, 2014b.

Hong Yang, Kaan Ozbay, and Kun Xie. Assessing the risk of secondary crashes on highways. *Journal of safety research*, 49:143–e1, 2014c.

William Yeoh and Makoto Yokoo. Distributed problem solving. *AI Magazine*, 33(3):53–53, 2012.

Yafeng Yin. Optimal fleet allocation of freeway service patrols. *Networks and Spatial Economics*, 6(3):221–234, 2006.

Yafeng Yin. A scenario-based model for fleet allocation of freeway service patrols. *Networks and Spatial Economics*, 8(4):407–417, 2008.

Makoto Yokoo and Katsutoshi Hirayama. Algorithms for distributed constraint satisfaction: A review. *Autonomous Agents and Multi-Agent Systems*, 3(2):185–207, 2000.

Soyoung Iris You, Joseph YJ Chow, and Stephen G Ritchie. Inverse vehicle routing for activity-based urban freight forecast modeling and city logistics. *Transportmetrica A: Transport Science*, 12(7):650–673, 2016.

Weixiong Zhang, Zhao Xing, Guandong Wang, and Lars Wittenburg. An analysis and application of distributed constraint satisfaction and optimization algorithms in sensor networks. In *AAMAS*, volume 3, pages 185–192. Citeseer, 2003.

APPENDIX

Publications, Presentations, Posters resulting from projects

1) Darko J., Park, H., A Proactive Dynamic-Distributed Constraint Opti-mization Framework for Unmanned Aerial and Ground Vehicles in TrafficIncident Managem. In: 2021 6th International Conference on IntelligentTransportation Engineering (ICITE 2021), 901, Springer Nature, Singa-pore Pte Ltd. 2022.

2) Darko, J., Park, H., Unmanned Aerial and Ground Emergency Vehicles in Traffic Incident Management: An Anticipatory Assignment Model. In 101th Annual Meeting of Transportation Research Board (TRB 2022), # 22-03332, Washington, DC, January, 2022.

3) Darko J., Folsom, L., Deshpande, N., Park, H., Distributed Constraint Optimization Problem for Coordinating Response of Unmanned Aerial Vehicles and Ground Vehicles. In 2021 5th Annual Conference of Information Sciences and Systems (CISS), 2021

4) Darko J., Folsom, L., Deshpande, N., Park, H., A new distributed agent framework for traffic incident management. In ASCE International Conference on Transportation & Development (ISTD2021), June, 2021.

5) Pugh N, Park H., High-Order Markov Model for Prediction of Secondary Crash Likelihood considering Incident Duration, Cogent Engineering, 8 (1). Taylor & Francis 2021

6) Darko J., Folsom, L., Park, H., DRONETIM: Dynamic Routing of Unmanned-aerial and Emergency Team Incident Management. In Transportation Science and Logistics Society, Second Triennial Conference, Arlington, VA, May 27-29, 2020

7) Darko J., Acquaah Y. Folsom, L., Park, H., Alden, A. DRONETIM: Dynamic Routing of Unmanned-aerial and Emergency Team Incident Management. In Proceedings of the 99th Annual Meeting of TRB2020, #20-02283, 2020.

8) Pugh N., Park, H., High-Order Markov Model for Prediction of Secondary Crash Likelihood Considering Incident Duration In Proceedings of the 99th Annual Meeting of TRB2020, #20-02092, 2020.

9) Pugh N, Park H., High-Order Markov Model for Prediction of Secondary Crash Likelihood Considering Incident Duration. Proceedings of the 99 th Annual Meeting of Transportation Research Board (tRb 2020), # 20-02092, Washington, DC, January 12–16, 2020.

10) Park H, Waddel D, Haghani A, Online emergency vehicle dispatching with look-ahead on a transportation network. Transportation Research Part C: Emerging Technologies, 109, 95-116. 2019.

11) Park H, Haghani A, Knodler M.A., Samuel S., Real-time crash prediction and avoidance under unexpected traffic congestion. Accident Analysis & Prevention, 112, 39-49. March, 2018.

Sample Crash Data

TMC	Severity	Start_Time	End_Time	Start_Lat	Start_Lng	Street	City	State
201	3	10/8/19 8:41	10/8/19 10:10	35.219238	-80.846565	South Blvd	Charlotte	NC
246	3	12/1/19 10:01	12/1/19 11:30	35.241058	-80.850662	I-77 N	Charlotte	NC
201	3	12/1/19 10:49	12/1/19 12:48	35.219238	-80.846565	South Blvd	Charlotte	NC
201	2	12/3/19 14:10	12/3/19 15:40	35.234428	-80.836815	I-77 N	Charlotte	NC
201	2	12/4/19 9:24	12/4/19 10:23	35.219238	-80.846565	South Blvd	Charlotte	NC
201	3	12/4/19 12:26	12/4/19 14:05	35.219528	-80.836212	S McDowell St	Charlotte	NC
201	2	12/4/19 12:34	12/4/19 14:49	35.227871	-80.847893	S Mint St	Charlotte	NC
343	2	12/5/19 7:31	12/5/19 10:02	35.23605	-80.839478	I-77 N	Charlotte	NC
201	3	12/6/19 14:55	12/6/19 16:27	35.219238	-80.846565	South Blvd	Charlotte	NC
201	2	12/6/19 17:10	12/6/19 18:10	35.22279	-80.833862	E 6th St	Charlotte	NC
201	2	12/7/19 11:05	12/7/19 12:34	35.241058	-80.850662	I-77 N	Charlotte	NC
201	2	12/7/19 11:31	12/7/19 12:45	35.216049	-80.846642	Euclid Ave	Charlotte	NC
201	3	12/9/19 16:28	12/9/19 17:28	35.213772	-80.844551	E Morehead St	Charlotte	NC
201	2	12/10/19 20:29	12/10/19 20:59	35.241058	-80.850662	I-77 N	Charlotte	NC
201	2	12/11/19 7:24	12/11/19 9:27	35.219528	-80.836212	S McDowell St	Charlotte	NC
201	3	12/11/19 15:53	12/11/19 16:38	35.241058	-80.850662	I-77 N	Charlotte	NC
201	2	12/12/19 6:14	12/12/19 6:44	35.227871	-80.847893	S Mint St	Charlotte	NC
201	2	12/12/19 22:27	12/12/19 22:57	35.241058	-80.850662	I-77 N	Charlotte	NC
201	2	12/13/19 8:08	12/13/19 9:47	35.221722	-80.848579	E Hill St	Charlotte	NC
201	2	12/18/19 10:12	12/18/19 10:42	35.213772	-80.844551	E Morehead St	Charlotte	NC
201	2	12/18/19 11:22	12/18/19 11:52	35.221279	-80.840271	S Davidson St	Charlotte	NC
201	2	12/23/19 10:46	12/23/19 11:49	35.219528	-80.836212	S McDowell St	Charlotte	NC
201	2	12/24/19 13:21	12/24/19 13:51	35.223789	-80.841187	E 4th St	Charlotte	NC
201	2	12/24/19 14:07	12/24/19 15:09	35.22607	-80.835732	N Caldwell St	Charlotte	NC
202	2	1/1/20 15:24	1/1/20 16:23	35.233913	-80.835983	I-77 N	Charlotte	NC
201	3	1/3/20 9:58	1/3/20 11:00	35.23547	-80.839355	Brookshire Fwy E	Charlotte	NC
201	3	1/6/20 9:17	1/6/20 12:17	35.233978	-80.836075	I-77 N	Charlotte	NC
201	2	1/7/20 8:27	1/7/20 10:26	35.217499	-80.847992	S Caldwell St	Charlotte	NC
201	2	1/9/20 8:00	1/9/20 8:44	35.223789	-80.841187	E 4th St	Charlotte	NC
241	3	1/10/20 7:15	1/10/20 9:02	35.241058	-80.850662	I-77 N	Charlotte	NC
201	3	1/13/20 8:49	1/13/20 9:41	35.241058	-80.850662	I-77 N	Charlotte	NC
201	2	1/14/20 14:55	1/14/20 16:09	35.241058	-80.850662	I-77 N	Charlotte	NC
201	2	1/15/20 7:49	1/15/20 9:38	35.219528	-80.836212	S McDowell St	Charlotte	NC
201	2	1/15/20 10:15	1/15/20 11:47	35.235352	-80.84259	W 9th St	Charlotte	NC
201	2	1/15/20 17:28	1/15/20 18:46	35.219528	-80.836212	S McDowell St	Charlotte	NC
201	2	1/15/20 18:52	1/15/20 19:52	35.227871	-80.847893	S Mint St	Charlotte	NC
245	3	1/17/20 6:42	1/17/20 8:41	35.241058	-80.850662	I-77 N	Charlotte	NC
201	2	1/17/20 8:43	1/17/20 11:00	35.213772	-80.844551	E Morehead St	Charlotte	NC
201	2	1/17/20 10:22	1/17/20 11:20	35.219238	-80.846565	South Blvd	Charlotte	NC
201	2	1/21/20 9:51	1/21/20 11:27	35.234516	-80.83696	Brookshire Fwy W	Charlotte	NC
201	2	1/22/20 8:33	1/22/20 9:34	35.228611	-80.846817	S Mint St	Charlotte	NC
201	3	1/22/20 9:09	1/22/20 10:10	35.234547	-80.837013	Brookshire Fwy W	Charlotte	NC
201	2	1/22/20 14:56	1/22/20 16:43	35.219238	-80.846565	South Blvd	Charlotte	NC
201	2	1/23/20 8:46	1/23/20 9:15	35.236134	-80.839417	N Graham St	Charlotte	NC
201	2	1/23/20 9:01	1/23/20 10:01	35.225761	-80.838287	E 5th St	Charlotte	NC
201	2	1/29/20 22:43	1/29/20 23:29	35.241058	-80.850662	I-77 N	Charlotte	NC
201	3	1/31/20 11:33	1/31/20 12:32	35.241058	-80.850662	I-77 N	Charlotte	NC
201	2	2/3/20 12:44	2/3/20 14:22	35.214779	-80.843102	Baxter St	Charlotte	NC

201	2	2/5/20 8:26	2/5/20 9:41	35.224411	-80.84948	W Stonewall St	Charlotte	NC
201	2	2/5/20 8:52	2/5/20 9:21	35.241058	-80.850662	I-77 N	Charlotte	NC
201	2	2/10/20 7:11	2/10/20 9:33	35.219528	-80.836212	S McDowell St	Charlotte	NC
201	2	2/11/20 8:25	2/11/20 9:10	35.223259	-80.83976	S Caldwell St	Charlotte	NC
201	2	2/11/20 8:33	2/11/20 10:14	35.229759	-80.848244	S Graham St	Charlotte	NC
201	2	2/11/20 8:42	2/11/20 10:12	35.241058	-80.850662	I-77 N	Charlotte	NC
241	2	2/12/20 6:03	2/12/20 7:04	35.213772	-80.844551	E Morehead St	Charlotte	NC
201	2	2/12/20 8:33	2/12/20 9:33	35.228611	-80.846817	S Mint St	Charlotte	NC
201	2	2/12/20 17:56	2/12/20 18:26	35.213772	-80.844551	E Morehead St	Charlotte	NC
201	3	2/13/20 15:37	2/13/20 16:22	35.241058	-80.850662	I-77 N	Charlotte	NC
201	2	2/13/20 20:26	2/13/20 22:33	35.241058	-80.850662	I-77 N	Charlotte	NC
246	3	2/13/20 20:38	2/13/20 23:00	35.241058	-80.850662	I-77 N	Charlotte	NC
201	2	2/14/20 8:47	2/14/20 10:03	35.226158	-80.837753	N Brevard St	Charlotte	NC
201	2	2/18/20 6:21	2/18/20 8:07	35.219528	-80.836212	S McDowell St	Charlotte	NC
201	2	2/20/20 18:24	2/20/20 19:24	35.229759	-80.848244	S Graham St	Charlotte	NC
201	2	2/20/20 19:01	2/20/20 19:46	35.219238	-80.846565	South Blvd	Charlotte	NC
201	2	2/20/20 20:58	2/20/20 23:16	35.23547	-80.839355	Brookshire Fwy E	Charlotte	NC
201	2	2/21/20 20:55	2/21/20 23:18	35.223751	-80.839027	S Caldwell St	Charlotte	NC
201	3	2/22/20 8:58	2/22/20 9:44	35.241058	-80.850662	I-77 N	Charlotte	NC
201	2	2/24/20 10:16	2/24/20 12:11	35.22744	-80.833771	N Caldwell St	Charlotte	NC
201	2	2/24/20 17:29	2/24/20 19:06	35.214779	-80.843102	Baxter St	Charlotte	NC
201	2	2/27/20 17:47	2/27/20 18:47	35.234432	-80.837067	Brookshire Fwy E	Charlotte	NC
201	2	2/27/20 17:48	2/27/20 18:48	35.23547	-80.839355	Brookshire Fwy E	Charlotte	NC
201	2	3/3/20 10:59	3/3/20 11:28	35.219238	-80.846565	South Blvd	Charlotte	NC
201	2	3/3/20 17:36	3/3/20 18:36	35.219238	-80.846565	South Blvd	Charlotte	NC
201	2	3/3/20 21:30	3/3/20 22:00	35.241058	-80.850662	I-77 N	Charlotte	NC
201	2	3/4/20 8:21	3/4/20 9:40	35.223751	-80.839027	S Caldwell St	Charlotte	NC
241	3	3/4/20 19:45	3/4/20 21:20	35.241058	-80.850662	I-77 N	Charlotte	NC
201	2	3/6/20 7:56	3/6/20 9:32	35.219528	-80.836212	S McDowell St	Charlotte	NC
201	2	3/7/20 13:09	3/7/20 13:53	35.225658	-80.845329	E 3rd St	Charlotte	NC
201	2	3/9/20 19:54	3/9/20 20:24	35.226158	-80.837753	N Brevard St	Charlotte	NC
201	2	3/11/20 9:36	3/11/20 10:23	35.241058	-80.850662	I-77 N	Charlotte	NC
201	2	3/12/20 8:32	3/12/20 9:01	35.241058	-80.850662	I-77 N	Charlotte	NC
201	2	3/13/20 6:01	3/13/20 9:22	35.22279	-80.833862	E 6th St	Charlotte	NC
201	2	3/16/20 10:31	3/16/20 11:01	35.219238	-80.846565	South Blvd	Charlotte	NC
201	2	3/17/20 8:53	3/17/20 9:23	35.233101	-80.855789	W 4th Street Ext	Charlotte	NC
201	2	3/24/20 15:05	3/24/20 18:28	35.223751	-80.839027	S Caldwell St	Charlotte	NC
245	3	3/25/20 19:44	3/25/20 20:13	35.241058	-80.850662	I-77 N	Charlotte	NC
201	2	4/9/20 10:24	4/9/20 11:24	35.241131	-80.850525	I-77 N	Charlotte	NC
201	2	4/10/20 16:36	4/10/20 19:21	35.241131	-80.850525	I-77 N	Charlotte	NC
201	2	4/11/20 9:40	4/11/20 10:42	35.220791	-80.848465	I-277 N	Charlotte	NC
201	3	4/12/20 16:42	4/12/20 17:27	35.241131	-80.850525	I-77 N	Charlotte	NC
201	2	4/13/20 16:26	4/13/20 17:25	35.23547	-80.839355	Brookshire Fwy E	Charlotte	NC
201	2	4/14/20 14:48	4/14/20 16:03	35.219444	-80.846817	South Blvd	Charlotte	NC
201	2	4/14/20 16:51	4/14/20 18:50	35.217499	-80.847992	S Caldwell St	Charlotte	NC
241	2	4/15/20 7:44	4/15/20 8:30	35.241131	-80.850525	I-77 N	Charlotte	NC
201	2	4/15/20 17:12	4/15/20 19:26	35.241131	-80.850525	I-77 N	Charlotte	NC
201	2	4/16/20 7:11	4/16/20 8:58	35.223789	-80.841187	E 4th St	Charlotte	NC

201	2	4/16/20 11:57	4/16/20 12:44	35.219444	-80.846817	South Blvd	Charlotte	NC
201	2	4/17/20 21:27	4/17/20 21:57	35.241131	-80.850525	I-77 N	Charlotte	NC
201	2	4/20/20 9:44	4/20/20 10:43	35.241131	-80.850525	I-77 N	Charlotte	NC
201	3	4/20/20 10:35	4/20/20 12:20	35.240833	-80.851021	I-77 S	Charlotte	NC
201	2	5/8/20 10:50	5/8/20 12:00	35.219528	-80.836212	S McDowell St	Charlotte	NC
201	2	5/18/20 7:42	5/18/20 9:03	35.219444	-80.846817	South Blvd	Charlotte	NC
246	3	5/18/20 20:05	5/18/20 21:15	35.241131	-80.850525	I-77 N	Charlotte	NC
201	2	5/22/20 7:36	5/22/20 9:03	35.227409	-80.847359	W 3rd St	Charlotte	NC
201	3	5/22/20 8:34	5/22/20 13:22	35.241131	-80.850525	I-77 N	Charlotte	NC
201	2	5/26/20 7:40	5/26/20 9:08	35.213772	-80.844551	E Morehead St	Charlotte	NC
244	2	6/2/20 6:58	6/2/20 7:41	35.23547	-80.839355	Brookshire Fwy E	Charlotte	NC
201	2	6/2/20 19:14	6/2/20 20:53	35.22607	-80.835732	N Caldwell St	Charlotte	NC
247	3	6/10/20 6:53	6/10/20 8:23	35.241131	-80.850525	I-77 N	Charlotte	NC
201	2	6/11/20 10:30	6/11/20 11:15	35.230591	-80.846977	Graham St	Charlotte	NC
201	3	6/11/20 15:45	6/11/20 16:13	35.23547	-80.839355	Brookshire Fwy E	Charlotte	NC
201	3	6/11/20 17:27	6/11/20 17:56	35.235847	-80.839264	I-77 N	Charlotte	NC
201	2	6/15/20 7:29	6/15/20 8:45	35.223991	-80.853058	I-277 S	Charlotte	NC
201	2	6/16/20 10:47	6/16/20 11:32	35.241131	-80.850525	I-77 N	Charlotte	NC
201	3	6/22/20 20:18	6/22/20 22:07	35.241131	-80.850525	I-77 N	Charlotte	NC
201	2	6/26/20 8:24	6/26/20 8:54	35.217499	-80.847992	S Caldwell St	Charlotte	NC
201	2	7/2/20 11:00	7/2/20 11:55	35.241131	-80.850525	I-77 N	Charlotte	NC
201	2	7/6/20 11:25	7/6/20 13:14	35.213772	-80.844551	E Morehead St	Charlotte	NC
201	2	7/21/20 21:58	7/21/20 23:16	35.241131	-80.850525	I-77 N	Charlotte	NC
201	2	7/23/20 9:52	7/23/20 10:52	35.219173	-80.847107	South Blvd	Charlotte	NC
245	3	7/23/20 14:56	7/23/20 15:25	35.241131	-80.850525	I-77 N	Charlotte	NC
241	3	7/30/20 13:04	7/30/20 13:49	35.241131	-80.850525	I-77 N	Charlotte	NC
201	2	8/11/20 6:46	8/11/20 9:30	35.22607	-80.835732	N Caldwell St	Charlotte	NC
201	2	8/12/20 12:58	8/12/20 13:27	35.217499	-80.847992	S Caldwell St	Charlotte	NC
201	2	8/12/20 18:29	8/12/20 19:29	35.241131	-80.850525	I-77 N	Charlotte	NC
241	2	8/12/20 18:30	8/12/20 19:30	35.22607	-80.835732	N Caldwell St	Charlotte	NC
201	2	8/14/20 10:07	8/14/20 10:37	35.219444	-80.846817	South Blvd	Charlotte	NC
241	3	8/15/20 21:40	8/15/20 22:09	35.241131	-80.850525	I-77 N	Charlotte	NC
201	3	8/18/20 12:36	8/18/20 15:21	35.241131	-80.850525	I-77 N	Charlotte	NC
201	2	8/21/20 4:03	8/21/20 5:08	35.219444	-80.846817	South Blvd	Charlotte	NC
201	3	8/22/20 14:27	8/22/20 15:28	35.241131	-80.850525	I-77 N	Charlotte	NC
201	2	8/24/20 11:53	8/24/20 12:38	35.219444	-80.846817	South Blvd	Charlotte	NC
201	3	8/26/20 16:35	8/26/20 17:37	35.241131	-80.850525	I-77 N	Charlotte	NC
201	2	8/29/20 10:04	8/29/20 11:25	35.219444	-80.846817	South Blvd	Charlotte	NC
201	2	9/1/20 9:27	9/1/20 12:19	35.23613	-80.839409	N Graham St	Charlotte	NC
201	2	9/4/20 19:26	9/4/20 20:28	35.224411	-80.84948	W Stonewall St	Charlotte	NC
245	3	9/9/20 14:49	9/9/20 16:35	35.241131	-80.850525	I-77 N	Charlotte	NC
201	3	9/9/20 16:58	9/9/20 18:15	35.241131	-80.850525	I-77 N	Charlotte	NC
201	2	9/14/20 16:12	9/14/20 17:14	35.241131	-80.850525	I-77 N	Charlotte	NC
201	2	9/17/20 5:05	9/17/20 6:38	35.219528	-80.836212	S McDowell St	Charlotte	NC
201	2	9/18/20 20:39	9/18/20 22:25	35.241131	-80.850525	I-77 N	Charlotte	NC
201	2	9/23/20 11:06	9/23/20 12:37	35.221279	-80.840271	S Davidson St	Charlotte	NC
201	2	9/24/20 7:48	9/24/20 8:48	35.235352	-80.84259	W 9th St	Charlotte	NC
201	2	9/24/20 17:18	9/24/20 18:28	35.241131	-80.850525	I-77 N	Charlotte	NC

241	1	10/10/20 16:31	10/10/20 18:11	35.225658	-80.845329	E 3rd St	Charlotte	NC
201	2	10/12/20 8:38	10/12/20 9:37	35.228168	-80.846298	S Poplar St	Charlotte	NC
201	2	10/21/20 10:11	10/21/20 11:26	35.223751	-80.839027	S Caldwell St	Charlotte	NC
201	2	10/22/20 11:21	10/22/20 12:20	35.22607	-80.835732	N Caldwell St	Charlotte	NC
201	2	10/23/20 17:31	10/23/20 18:31	35.229759	-80.848244	S Graham St	Charlotte	NC
241	2	10/29/20 17:39	10/29/20 18:43	35.219578	-80.84716	I-277 N	Charlotte	NC
201	2	10/30/20 10:27	10/30/20 11:57	35.230591	-80.846977	Graham St	Charlotte	NC
241	2	11/3/20 16:44	11/3/20 17:45	35.22945	-80.84568	W Trade St	Charlotte	NC
201	2	11/3/20 18:41	11/3/20 19:47	35.230591	-80.846977	Graham St	Charlotte	NC
201	2	11/4/20 9:22	11/4/20 10:51	35.223789	-80.841187	E 4th St	Charlotte	NC
241	2	11/4/20 16:43	11/4/20 17:43	35.219528	-80.836212	S McDowell St	Charlotte	NC
241	2	11/6/20 13:08	11/6/20 13:38	35.217499	-80.847992	S Caldwell St	Charlotte	NC
241	2	11/6/20 14:13	11/6/20 15:58	35.223751	-80.839027	S Caldwell St	Charlotte	NC
241	3	11/9/20 17:53	11/9/20 18:52	35.219578	-80.84716	I-277 N	Charlotte	NC
241	2	11/10/20 18:52	11/10/20 19:21	35.223751	-80.839027	S Caldwell St	Charlotte	NC
201	2	11/13/20 7:15	11/13/20 7:42	35.223751	-80.839027	S Caldwell St	Charlotte	NC
246	3	11/20/20 15:37	11/20/20 16:50	35.239857	-80.851807	I-77 N	Charlotte	NC
201	2	12/17/20 18:20	12/17/20 19:19	35.22607	-80.835732	N Caldwell St	Charlotte	NC
241	2	12/18/20 6:14	12/18/20 6:58	35.219578	-80.84716	I-277 N	Charlotte	NC
241	2	12/18/20 19:31	12/18/20 20:34	35.227871	-80.847893	S Mint St	Charlotte	NC
201	3	10/7/19 13:09	10/7/19 14:38	35.21759	-80.871803	I-77 N	Charlotte	NC
244	3	10/9/19 14:16	10/9/19 15:46	35.209557	-80.875587	I-77 S	Charlotte	NC
241	2	12/2/19 10:00	12/2/19 11:27	35.205559	-80.869469	S Tryon St	Charlotte	NC
201	2	12/2/19 15:25	12/2/19 17:27	35.206661	-80.870659	Baltimore Ave	Charlotte	NC
201	2	12/4/19 16:36	12/4/19 18:06	35.205559	-80.869469	S Tryon St	Charlotte	NC
247	3	12/11/19 6:39	12/11/19 7:09	35.209557	-80.875587	I-77 S	Charlotte	NC
241	3	12/12/19 21:44	12/12/19 23:27	35.209557	-80.875587	I-77 S	Charlotte	NC
201	2	12/18/19 8:43	12/18/19 11:54	35.205559	-80.869469	S Tryon St	Charlotte	NC
201	2	12/19/19 15:11	12/19/19 15:41	35.205559	-80.869469	S Tryon St	Charlotte	NC
201	3	12/24/19 12:36	12/24/19 13:52	35.209557	-80.875587	I-77 S	Charlotte	NC
201	2	12/29/19 15:50	12/29/19 16:51	35.22002	-80.852127	S College St	Charlotte	NC
201	3	1/2/20 14:10	1/2/20 15:28	35.209557	-80.875587	I-77 S	Charlotte	NC
201	2	1/3/20 8:11	1/3/20 10:03	35.20546	-80.839569	Romany Rd	Charlotte	NC
201	3	1/3/20 8:51	1/3/20 10:58	35.209557	-80.875587	I-77 S	Charlotte	NC
201	3	1/3/20 13:38	1/3/20 14:23	35.209557	-80.875587	I-77 S	Charlotte	NC
201	2	1/7/20 14:28	1/7/20 16:46	35.209557	-80.875587	I-77 S	Charlotte	NC
247	3	1/8/20 6:53	1/8/20 8:26	35.209557	-80.875587	I-77 S	Charlotte	NC
343	3	1/8/20 7:13	1/8/20 7:58	35.209557	-80.875587	I-77 S	Charlotte	NC
247	3	1/8/20 9:55	1/8/20 10:54	35.21019	-80.874985	I-77 N	Charlotte	NC
201	3	1/9/20 11:38	1/9/20 12:38	35.209557	-80.875587	I-77 S	Charlotte	NC
201	3	1/17/20 7:14	1/17/20 7:43	35.209557	-80.875587	I-77 S	Charlotte	NC
201	3	1/21/20 16:04	1/21/20 16:33	35.209557	-80.875587	I-77 S	Charlotte	NC
201	3	1/25/20 19:41	1/25/20 21:34	35.209557	-80.875587	I-77 S	Charlotte	NC
201	2	1/28/20 9:18	1/28/20 10:33	35.224159	-80.854424	W Morehead St	Charlotte	NC
201	2	1/30/20 8:57	1/30/20 10:28	35.220409	-80.850616	S College St	Charlotte	NC
201	2	2/3/20 8:39	2/3/20 9:09	35.203159	-80.869469	Brelade Pl	Charlotte	NC
247	2	2/5/20 7:08	2/5/20 10:00	35.221779	-80.852112	Winnifred St	Charlotte	NC
201	2	2/6/20 9:46	2/6/20 10:34	35.219028	-80.851936	E Carson Blvd	Charlotte	NC
201	2	2/7/20 8:40	2/7/20 9:27	35.203011	-80.83744	Medical Center Dr	Charlotte	NC

241	3	2/14/20 19:24	2/14/20 20:42	35.209557	-80.875587	I-77 S	Charlotte	NC
201	2	2/21/20 9:58	2/21/20 11:44	35.209557	-80.875587	I-77 S	Charlotte	NC
201	3	2/25/20 7:12	2/25/20 7:57	35.218407	-80.871681	I-77 N	Charlotte	NC
201	3	2/25/20 19:16	2/25/20 20:56	35.218056	-80.871643	I-77 N	Charlotte	NC
201	2	2/27/20 8:51	2/27/20 10:05	35.220409	-80.850616	S College St	Charlotte	NC
201	3	2/28/20 14:40	2/28/20 15:10	35.209557	-80.875587	I-77 S	Charlotte	NC
247	2	3/4/20 9:17	3/4/20 10:01	35.209557	-80.875587	I-77 S	Charlotte	NC
201	2	3/5/20 7:16	3/5/20 9:22	35.209557	-80.875587	I-77 S	Charlotte	NC
201	2	3/9/20 13:22	3/9/20 14:51	35.220409	-80.850616	S College St	Charlotte	NC
201	2	3/12/20 17:59	3/12/20 19:17	35.205559	-80.869469	S Tryon St	Charlotte	NC
201	2	3/17/20 13:09	3/17/20 14:38	35.209557	-80.875587	I-77 S	Charlotte	NC
201	2	3/20/20 17:35	3/20/20 18:52	35.209557	-80.875587	I-77 S	Charlotte	NC
201	2	3/26/20 18:33	3/26/20 19:32	35.218334	-80.871529	I-77 N	Charlotte	NC
201	2	4/3/20 9:32	4/3/20 10:50	35.203011	-80.83744	Medical Center Dr	Charlotte	NC
201	2	4/3/20 12:55	4/3/20 14:24	35.209557	-80.875587	I-77 S	Charlotte	NC
201	2	4/7/20 13:01	4/7/20 13:48	35.214241	-80.878891	Remount Rd	Charlotte	NC
201	2	4/17/20 10:18	4/17/20 11:51	35.209557	-80.875587	I-77 S	Charlotte	NC
201	2	4/21/20 17:05	4/21/20 18:35	35.209557	-80.875587	I-77 S	Charlotte	NC
201	2	4/22/20 17:39	4/22/20 19:09	35.214241	-80.878891	Remount Rd	Charlotte	NC
201	2	4/30/20 8:54	4/30/20 9:55	35.205559	-80.869469	S Tryon St	Charlotte	NC
201	2	5/1/20 14:46	5/1/20 15:16	35.209557	-80.875587	I-77 S	Charlotte	NC
201	2	5/7/20 6:47	5/7/20 7:50	35.220409	-80.850616	S College St	Charlotte	NC
201	2	5/19/20 6:16	5/19/20 7:30	35.209557	-80.875587	I-77 S	Charlotte	NC
201	2	5/19/20 7:42	5/19/20 8:11	35.209557	-80.875587	I-77 S	Charlotte	NC
241	2	5/25/20 15:38	5/25/20 16:43	35.209557	-80.875587	I-77 S	Charlotte	NC
201	2	5/28/20 11:27	5/28/20 12:27	35.209557	-80.875587	I-77 S	Charlotte	NC
201	3	6/3/20 19:35	6/3/20 20:34	35.212227	-80.873909	I-77 N	Charlotte	NC
201	4	6/11/20 10:52	6/11/20 19:22	35.209736	-80.87545	I-77 S	Charlotte	NC
201	2	6/22/20 9:50	6/22/20 10:40	35.209557	-80.875587	I-77 S	Charlotte	NC
244	2	7/16/20 8:01	7/16/20 8:46	35.217987	-80.871857	I-77 N	Charlotte	NC
201	3	7/16/20 18:41	7/16/20 19:10	35.209557	-80.875587	I-77 S	Charlotte	NC
201	2	7/16/20 18:41	7/16/20 19:41	35.209	-80.873878	Remount Rd	Charlotte	NC
201	2	7/17/20 19:38	7/17/20 21:56	35.201099	-80.869003	Fairwood Ave	Charlotte	NC
201	2	7/20/20 16:31	7/20/20 17:46	35.214241	-80.878891	Remount Rd	Charlotte	NC
201	2	7/22/20 7:56	7/22/20 8:56	35.20676	-80.859001	Euclid Ave	Charlotte	NC
201	3	7/23/20 9:36	7/23/20 10:21	35.209557	-80.875587	I-77 S	Charlotte	NC
201	2	7/24/20 8:00	7/24/20 10:03	35.209557	-80.875587	I-77 S	Charlotte	NC
201	2	8/6/20 6:59	8/6/20 8:28	35.218563	-80.848831	E Morehead St	Charlotte	NC
201	2	8/10/20 18:41	8/10/20 20:15	35.209557	-80.875587	I-77 S	Charlotte	NC
201	3	8/11/20 5:55	8/11/20 7:26	35.209557	-80.875587	I-77 S	Charlotte	NC
201	2	8/11/20 14:41	8/11/20 15:11	35.205559	-80.869469	S Tryon St	Charlotte	NC
201	2	8/21/20 8:46	8/21/20 10:50	35.220409	-80.850616	S College St	Charlotte	NC
201	2	8/25/20 10:28	8/25/20 12:17	35.220409	-80.850616	S College St	Charlotte	NC
201	2	9/3/20 7:52	9/3/20 8:45	35.209557	-80.875587	I-77 S	Charlotte	NC
241	3	9/14/20 16:45	9/14/20 17:29	35.209557	-80.875587	I-77 S	Charlotte	NC
201	2	9/22/20 10:57	9/22/20 12:11	35.205559	-80.869469	S Tryon St	Charlotte	NC
201	3	9/24/20 18:30	9/24/20 19:46	35.209557	-80.875587	I-77 S	Charlotte	NC
201	3	9/30/20 8:43	9/30/20 9:30	35.218452	-80.871658	I-77 N	Charlotte	NC